Investigation of the chemical changes during the thermal treatment of acrylonitrile co methyl acrylate-polymer (polyacrylonitrile precursor) focusing on the fate of the methyl acrylate moiety

Klaus Ruhland, Robert Horny, Andrea Wanzel, Sebastian Reisach, Alina Nizamutdinova, Holger Kirchhain, Ulrich Rehfuss, Leo van Wüllen, Andreas Fischer, Felix Scheliga, Tobias Hübner

Angaben zur Veröffentlichung / Publication details:

Ruhland, Klaus, Robert Horny, Andrea Wanzel, Sebastian Reisach, Alina Nizamutdinova, Holger Kirchhain, Ulrich Rehfuss, et al. 2022. "Investigation of the chemical changes during the thermal treatment of acrylonitrile co methyl acrylate-polymer (polyacrylonitrile precursor) focusing on the fate of the methyl acrylate moiety." *Journal of Applied Polymer Science* 139 (18): 52074. https://doi.org/10.1002/app.52074.

Received: 29 October 2021 | Revised: 3 December 2021 | Accepted: 8 December 2021

DOI: 10.1002/app.52074

ARTICLE

Applied Polymer SCIENCE WILEY

Investigation of the chemical changes during the thermal treatment of acrylonitrile-co-methyl acrylate-polymer (polyacrylonitrile-precursor) focusing on the fate of the methyl acrylate moiety

Klaus Ruhland[1] | **Robert Horny**[2] | **Andrea Wanzel**[1] | **Sebastian Reisach**[2] | **Alina Nizamutdinova**[1] | **Holger Kirchhain**[1] | **Ulrich Rehfuss**[1] | **Leo van Wüllen**[1] | **Andreas Fischer**[1] | **Felix Scheliga**[3] | **Tobias Hübner**[2]

[1]Institute of Physics, Chemical Physics and Materials Science, University of Augsburg, Augsburg, Germany

[2]Institute of Materials Resource Management, University of Augsburg, Augsburg, Germany

[3]Institute of Technical and Macromolecular Chemistry, University of Hamburg, Hamburg

Correspondence
Klaus Ruhland, Institute of Physics, Chemical Physics and Materials Science, University of Augsburg, Universitätsstr. 1 D-86135 Augsburg, Germany.
Email: klaus.ruhland@physik.uni-augsburg.de

Abstract

Seventeen samples of acrylonitrile (AN)-co-methyl acrylate (MA)-polymer (MA content 0–11 mol%) are examined. Several selective isotopic labelings are employed (d^1-MA, d^2-MA, ^{13}CO-MA, CD_3-MA, d^1-AN, d^2-AN, and ^{15}N-AN). The thermal treatment under inert atmosphere is investigated to gain insight into the chemical transformation mechanisms concerning the MA sub-unit. The volatiles are determined by means of evolved gas analysis (EGA) (Fourier transform infrared [FTIR] and GC/MS). Methanol is found for the first time as one decisive volatile stemming from the MA sub-unit, next to water and carbon dioxide. In addition, methylamines are proven to be formed by reaction of ammonia with the MA sub-unit, while a similar reaction of hydrogen cyanide (HCN) yielding in acetonitrile could be ruled out. Several volatile compounds could even be quantified. The non-volatile polymeric material is characterized by means of simultaneous thermal analysis (differential scanning calorimetry, thermogravimetric analysis), in-situ-FTIR spectroscopy and sophisticated solid-state NMR methods. Selected defined model compounds are synthesized and analyzed for comparison. Detailed reaction mechanisms for the thermal transformation are concluded from the results, pointing in particular to the importance of ammonia for all processes as stoichiometric and/or catalytic reagent.

KEYWORDS

copolymers, degradation, radical polymerization, spectroscopy, thermogravimetric analysis

1 | INTRODUCTION

Polyacrylonitrile (PAN) represents by far the most important precursor material to fabricate high tensile carbon fibers (CF).[1,2] The manufacturing process is complex, including the drawing of the PAN fiber followed by the thermal treatment of the generated precursor fiber under different atmospheres at different temperatures. Since at different stages of the fabrication different challenges are set onto the properties of the material, beside of the main monomer acrylonitrile (AN) small amounts of comonomers such as acrylic acid,[3–6] methacrylic acid,[7] itaconic acid,[8–10] methyl methacrylate,[11] or methyl acrylate (MA)[12–20] are introduced into the PAN precursor each of which improving the performance at different stages within the process of CF manufacturing in comparison to the PAN homopolymer (Figure 1).

According to previous examinations in particular two large groups of comonomers can be distinguished: Firstly, those that support physical properties such as the glass transition temperature, melting temperature and transport phenomena within the fiber during the drawing process (influencing solvent diffusion and solubility) and during the thermal stabilization (influencing air permeation ⇒ acrylic esters; no mobile acidic hydrogen), and secondly, those influencing the chemical transformations during the thermal stabilization step (free carboxylic acids; mobile acidic hydrogens).

Methyl acrylate (MA) is the most important comonomer applied to promote the drawing process of the precursor fiber. Several papers have been published about the influence of this comonomer on the chemical changes during the thermal treatment of the AN-co-MA-copolymer. A first series of papers was published by Simitzis[12,13] in 1977. He examined the composition of volatiles during pyrolysis under Helium atmosphere of PAN fibers with 1% and 5% MA via gas chromatography. No methanol was found in his experiments. No comment is given on how the content of MA in the copolymer was determined. According to his results, the ester group of MA is decomposed only at temperatures higher than 400°C. No comment is given on how this occurs. Thermogravimetry was performed under an N_2 atmosphere. It was found that the weight loss of copolymer in the temperature range of the stabilization (280–300°C at 10°C/min heating rate) was smaller as compared to the PAN homopolymer. Via differential thermal analysis (DTA) under air, it was concluded that the onset temperature for the stabilization is almost independent of the MA content while the peak area decreases with increasing amount of MA. It was derived from the results that the MA units cause a catalytic action on the cyclization reaction. In 1993, Bhat published a paper including the performance of PAN containing 2% of MA under N_2 atmosphere, examined via differential scanning calorimetry (DSC; heating rate: 20°C/min).[14] No comment was given on how the content of MA was determined. In their examinations, the MA-containing copolymer showed the exothermic stabilization peak at slightly lower temperatures as compared to the PAN homopolymer. In 1994, a publication of H. Ogawa described the stabilization behavior of PAN fibers with different amounts of MA between 2% and 10%.[15] He concentrated his examinations on macroscopic properties such as shrinkage, oxygen content in the sample and carbonization yield. Chemical mechanistic conclusions were not drawn. In 1998, a paper was published by H. H. Cho about the effect of MA content (0%–6%) on the micro-structural changes of PAN copolymer during thermal treatment in the presence of air.[16] The MA content was determined by means of IR spectroscopy although the oscillation strength ratio between the nitrile stretching vibration and the carbonyl stretching vibration, which was used for the quantification, was not cited in this paper. They, for the first time, mentioned that the MA unit interferes with, rather than supports the cyclization reaction. This was concluded by their DSC measurements (heating rate and atmosphere not mentioned) in which the onset of cyclization increases with increasing MA content. No chemical mechanistic conclusions were drawn about the action of the MA unit concerning the stabilization behavior. In a triad of papers between 2002 and 2003 the authors Baird, McGrath and Wilkes examined the influence of MA

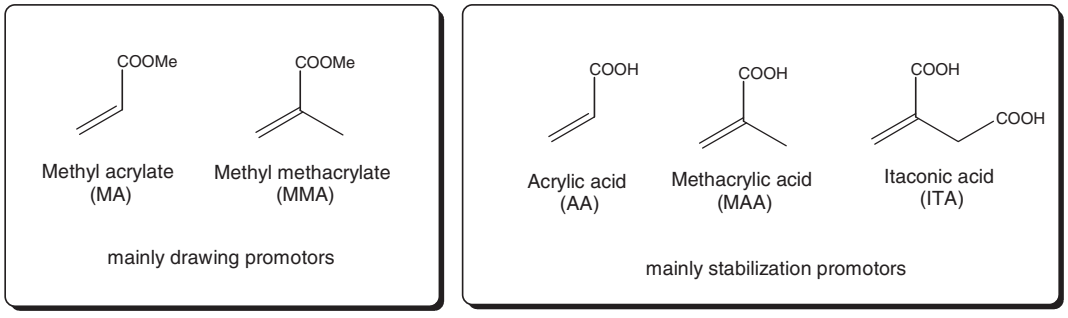

FIGURE 1 Comonomers used to improve the performance of polyacrylonitrile within the carbon fiber production process

content in particular on the melting behavior of the PAN copolymer (MA content between 0% and 15% determined by ^{1}H NMR spectroscopy).[17–19] They performed DTA measurements under N_2 atmosphere (heating rate 60°C/min) and could confirm that with increasing amount of MA the onset temperature for the stabilization increases while the peak area decreases, supporting the inhibiting character of MA for the stabilization/cyclization process. No explanation or chemical mechanistic conclusion was provided for this finding. In 2013 a paper was published by the group of Zhou who examined a commercial PAN fiber containing 1.0% of MA (determination method not mentioned) by means of DSC, thermogravimetric analysis (TGA), in situ-FTIR and solid-state NMR spectroscopy under an atmosphere of air in the temperature range between room temperature and 320°C. They concluded that the MA moiety acts as an initiator for the cyclization reaction of the nitrile moieties at lower temperatures (69–223°C). A clear, complete and convincing chemical pathway for this initiation step was not proposed..[20]

We herein report our results about the performance of the comonomer methyl acrylate (MA), respectively its smallest repeat unit, during the thermal treatment of the copolymer under inert atmosphere. We point out that the real industrial thermal treatment is performed under air, which will further complicate the reaction pathways. However, even under inert conditions, the description is very complex, and thus it is reasonable to first put the at least more defined purely thermal behavior under inert atmosphere on safer ground.

We used 17 self-synthesized AN-co-MA-polymer powders with different amounts of MA content (0%–11% by FTIR determination) as starting materials, including several selectively isotopically labeled monomers (d^1-MA, d^2-MA, ^{13}CO-MA, CD_3-MA, d^1-AN, d^2-AN, ^{15}N-AN, and ^{15}N-acrylamide [AAM]; all isotopically labeled monomers were self-synthesized; the reason for the usage of acrylamide will become clear during the discussion of the results). The key examinations were performed by means of EGA for the volatile compounds formed (FTIR and GC/MS) and by means of DSC, TGA, in-situ-FTIR spectroscopy and solid-state NMR spectroscopy of selected samples for the residing bulk material. Additionally, defined model compounds have been synthesized, analyzed and treated thermally for comparison.

Our focus was set in particular on the fate of the MA moiety. We could, for the first time, prove and quantify that a major amount of the methoxy groups leaves the material as methanol at the beginning of the thermal transformation under inert gas atmosphere, and by taking into account the results concerning the isotopically labeled materials we could sharpen the chemical pathways on which the methanol is formed. We propose that ammonia plays a crucial role in all transformation reactions concerning the MA sub-unit as catalyst or initiator or both. Other volatile compounds formed from the MA unit are CO_2 and H_2O, which were also quantified and, less obviously, methylamines. Acetonitrile on the other hand was proven not to be formed by reaction of HCN with the methyl group of the MA unit (Krapcho-type reaction). Detailed formation mechanisms for the volatiles are proposed. Also, evidence for the importance of hydrogen bonding of the in principle highly volatile ammonia to the solid polymeric material is given for the first time. A single semi-quantitative reaction scheme summing up to an explanation for the chemical transformations of more than 90% of all MA units is finally proposed and an explanation for the inhibiting character of the MA unit on the classical thermal transformation of PAN (cyclization/stabilization) is provided.

2 | EXPERIMENTAL

2.1 | Samples' synthesis, preparation, and characterization

2.1.1 | Monomer synthesis

In this work, we used several self-synthesized isotopically labeled monomers for the sample preparation (Figure 2).

^{15}N-AAM, ^{15}N-AN, and CD_3-MA have been synthesized according to previously published procedures.[21,22] The other isotopically labeled monomers were synthesized according to the reaction pathways presented in Figure 3.

Experimental details of the synthesis and the characterization data of the compounds are provided in the Figure SI1. An alternative synthesis for d^1-AN has been described in the literature.[23] In our hands this procedure turned out not to be confidently reproducible and, thus, we recommend our synthesis way.

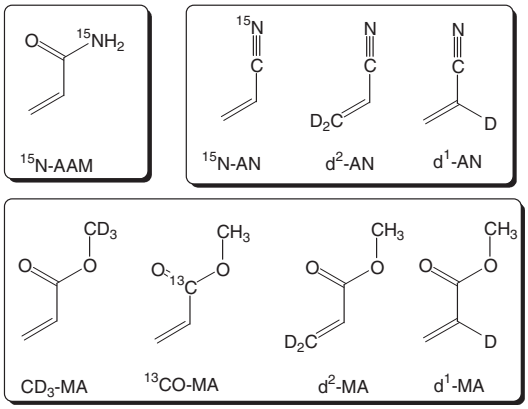

FIGURE 2 Isotopically labeled monomers used in this study

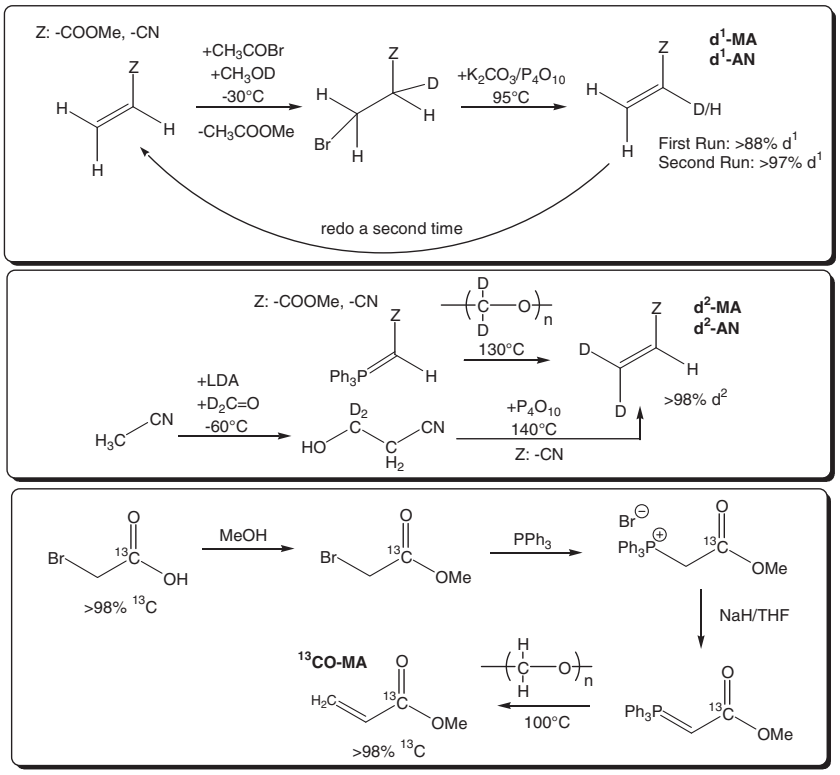

FIGURE 3 Synthesis reactions for the isotopically labeled monomers

TABLE 1 Characterization data for the copolymer samples applied in this study

Sample	Isotopic labeling	MA content (FTIR) (mol%)	AAM content (^{1}H NMR) (mol%)	P_n (SEC)	P_n (^{1}H NMR)	$Đ$ (SEC)
P1	–	0.7 ± 0.04	–	190 ± 10	177 ± 27	2.1
P2	–	1.9 ± 0.1	–	189 ± 9	172 ± 26	2.3
P3	–	2.9 ± 0.1	–	191 ± 10	185 ± 28	2.0
P4	–	4.4 ± 0.2	–	232 ± 12	212 ± 32	2.0
P5	–	5.1 ± 0.3	–	198 ± 10	187 ± 28	2.0
P6	–	8.0 ± 0.4	–	236 ± 12	223 ± 33	1.9
P7	–	9.0 ± 0.5	–	204 ± 10	226 ± 34	2.1
P8	–	11.2 ± 0.6	–	211 ± 11	212 ± 32	2.1
P9	CD_3-MA	4.5 ± 0.2	–	183 ± 9	181 ± 27	2.0
P10	d^1-AN	5.4 ± 0.3	–	201 ± 10	249 ± 50	2.3
P11	d^2-AN	6.8 ± 0.3	–	136 ± 7	129 ± 26	1.9
P12	d^1-MA	9.4 ± 0.5	–	191 ± 10	218 ± 33	2.1
P13	d^2-MA	11.0 ± 0.6	–	190 ± 10	201 ± 30	2.1
P14	d^2-MA	6.7 ± 0.3	–	185 ± 10	191 ± 29	2.0
P15	d^1-AN, d^1-MA	7.8 ± 0.4	–	208 ± 10	238 ± 48	2.3
P16	^{15}N-AN, CD_3-MA	6.0 ± 0.3	–	183 ± 9	201 ± 28	2.0
P17	^{15}N-AN, ^{13}CO-MA	10.1 ± 0.7	–	204 ± 10	211 ± 30	2.0
P18	^{15}N-AAM	–	9.2 ± 0.9	175 ± 9	182 ± 27	1.9
P19	^{15}N-AAM	6.9 ± 0.3	4.3 ± 0.7	180 ± 9	191 ± 26	2.0

From the non-labeled commercial monomers AN and MA the inhibitors were removed by extraction with aqueous NaOH followed by drying with $MgSO_4$ and distillation. All monomers were degassed by three freeze/pump/thaw cycles under argon and stored at −30°C prior to their use.

2.1.2 | Polymerization

The copolymers were prepared by free radical solution polymerization in dimethyl formamide (DMF) using azo-isobutyronitrile (AIBN) as thermal initiator. Experimental details of the synthesis are described in the Figure SI2. In total 17 different (AN-co-MA)-polymers were investigated differing in the content of MA comonomer and the isotopic labeling of the material (Table 1). Additionally, two samples containing ^{15}N-AAM were examined for reasons explained below.

2.1.3 | Characterization of the starting material

Since we are applying self-synthesized starting materials, we are able to provide a scientifically clear statement about their composition. The copolymer powders were characterized by means of FTIR spectroscopy, ^{1}H NMR spectroscopy (in case of labeled compounds also ^{2}H, ^{13}C and ^{15}N NMR [solution as well as solid state]), size exclusion chromatography (SEC) and X-ray powder diffractometry (XRD). For some experiments, a separation according to the mesh size of the polymer powder was done by means of a micro sieve tower with five mesh sizes between 50 μm and 1 mm to examine the influence of surface area on the chemical transformations during the thermal treatment. The relative content of incorporated MA comonomer was determined by means of FTIR spectroscopy and ^{1}H NMR spectroscopy. The FTIR spectroscopic evaluation was performed based on the ratio of the absorbances of the ν(C═O) stretching vibration at 1732 cm^{-1} and of the ν(C≡N) stretching vibration at 2242 cm^{-1}. To account for different oscillation strengths of the two vibrations a calibration with liquid mixtures of different defined amounts of methyl isobutyrate (1737 cm^{-1}) and isobutyronitrile (2245 cm^{-1}) was performed, and the ratio of the oscillation strength was found to be 26.648 (R^2 = 0.9996; see also Figure SI3). According to our evaluation, FTIR spectroscopy is the most trustable method to determine the content of MA. A small error of this method arises from the fact that in all samples traces of DMF were still present despite of washing with water and drying the powders in vacuo at 60°C (DMF is the solvent during the polymer synthesis; the residual amount is less than 1 mol%; the residual DMF evaporates from the sample prior to the thermally initiated changes in the polymer, as proven by EGA measurement (see Figure SI4), and does not interfere with or contribute to the chemical changes discussed in this paper). The ν(C═O) peak of DMF appears at 1660 cm^{-1} and, thus, slightly overlaps with the signal for incorporated MA at the base line (a ratio of oscillation strength ν(C═O; DMF)/ν(C≡N; isobutyronitrile) = 48.0 was estimated via IR calibration with defined mixtures of DMF and isobutyronitrile; R^2 = 0.990). For P17 with ^{13}C labeled carbonyl group (shift of the ν(C═O) wave number from 1732 to 1687 cm^{-1}) this problem becomes serious and the MA content of this sample is most likely slightly overestimated because of the overlay with the DMF peak (although not much, as we can prove by comparison with the ^{1}H NMR results).

The content of MA in the copolymer can also be determined by means of ^{1}H NMR spectroscopy using the ratio between the signal area for the CH^{AN} groups and/or the $CH_2{}^{AN}$ groups of AN in the polymer backbone and the signal area for the $CH_3{}^{MA}$ group of MA (Figure 4).

However, this is connected with serious problems, because while the signal area of the $CH_3{}^{MA}$ groups is quite narrow (at about 3.67 ppm) the signal areas of the CH groups and CH_2 groups are very broad with pronounced tailing on both sides (the signal area of $CH_2{}^{MA}$ partly overlaps with the one of $CH_2{}^{AN}$) which causes severe difficulties for an accurate integration. Due to these aspects, the MA content determination is less accurate based on ^{1}H NMR spectroscopy as compared to the IR measurement, although the results of the two methods correspond quite well with each other when using the integral of the $CH_3{}^{MA}$ group and the peak area for the CH^{AN} groups (see Figure SI6). In this publication when we draw conclusions about the influence of the MA content, we will always refer to the values determined by means of FTIR spectroscopy.

The measured MA content in the polymeric sample can be confidently pre-calculated from the weighted-in amount of MA applying our synthesis conditions by a constant factor of 0.767 for the non-deuterated samples (R^2 = 0.996; see also Figure SI7). This factor also works well for sample P17, showing (together with the ^{1}H NMR results) that the systematic error caused by DMF is small.

Several deuterated samples deviate significantly from this quite confident correlation giving evidence for a secondary kinetic isotopic effect during the radical polymerization for d^1-AN, d^2-AN and d^1-MA, while d^2-MA and d^3-MA did not show a deviation; see Figures SI7 and SI8).

Because of the small amounts, the chemical shift ranges of CH^{MA} and $CH_2{}^{MA}$, indicated in Figure 4, can only be guessed from the ^{1}H NMR measurement. They were unequivocally determined by means of ^{2}H NMR spectroscopy of samples, P12 and P13 (see Figure SI5). ^{2}H-{^{1}H} CPMAS solid-state NMR measurements have been performed with samples P9, P10, P11, and P16 (spectra see Figure 15 and Figure SI9) and quadrupole coupling constants of 160 ± 6 kHz for CD^{AN}, 162

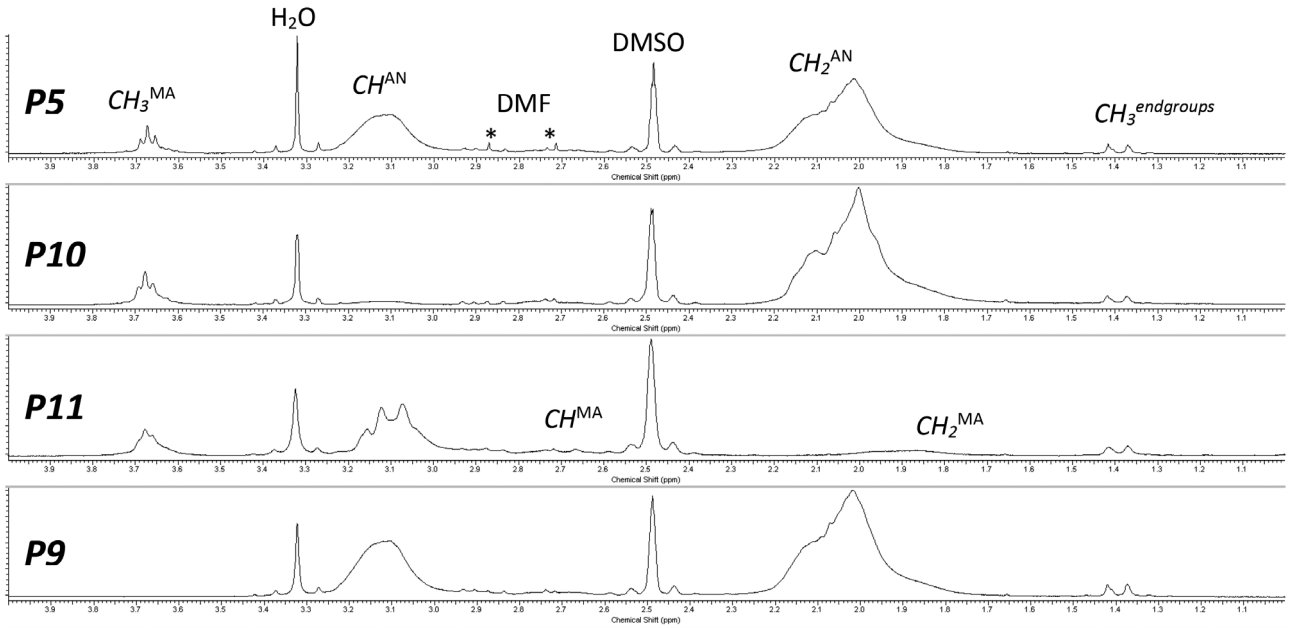

FIGURE 4 ^{1}H NMR spectra of samples P5, P9, P10, and P11 (the chemical shift area of the CH^{MA} and $CH_2{}^{MA}$ protons was derived from the ^{2}H NMR spectra of P12 and P13 (see Figure SI5)

$\pm$ 6 kHz for $CD_2{}^{AN}$ and 52 $\pm$ 6 kHz for $CD_3{}^{MA}$ were extracted demonstrating the expected higher mobility of the side-chain $CD_3{}^{MA}$ group as compared to the backbone CD^{AN} and $CD_2{}^{AN}$ moieties. For samples P16 and P17 the ^{15}N-labeled nitriles show up as a group of peaks between −126.4 and −123.4 ppm in ^{15}N NMR spectroscopy. The wavenumber of the ν(C≡N) stretching vibration shows the expected isotopic shift from 2242 to 2215 cm^{-1}. For sample P17 the ^{13}CO signal in ^{13}C NMR spectroscopy is found as a group of peaks between 173.5 and 174.8 ppm (isotopic shift of the wavenumber in IR spectroscopy from 1732 to 1687 cm^{-1}; chemical shifts for the other functionalities in ^{13}C NMR spectroscopy: 119.9–121.3 ppm (CN^{AN}), 52.2–52.6 ($CH_3{}^{MA}$), 33.8–34.6 ppm (CH^{MA}), 32.6–33.5 (CH^{AN}), 27.0–28.4 ppm ($CH_2{}^{AN}$), 26.0–26.6 ($CH_2{}^{MA}$)).

In contrast to the MA content the AAM content is more accurately determined by means of ^{1}H NMR spectroscopy comparing the integral of the NH protons (two broad multipletts at 7.17 and 7.75 ppm, $^{1}J_{NH}$ = 88 Hz) with the integral of the CH protons. A quantification by means of FTIR spectroscopy is complicated by concentration-dependent H-bonds, and a simple linear calibration curve for the amide carbonyl bands cannot be expected and was not found using defined mixtures of isobutyronitrile with acetamide. In ^{13}C NMR spectroscopy the amide, carbonyl carbons show up as a group of peaks between 174.0 and 175.0 ppm in DMSO-d^{6} solution. The ^{15}N NMR signals for the amide moiety are found between −265 ppm and −267 ppm.

The molecular weight distribution and the average degree of polymerization of the polymer samples were determined by means of size exclusion chromatography (SEC; Table 1; chromatograms see Figure SI10). The evaluation was done versus polystyrene standards. The reproducibility of these results was found to be ±5%. The data were corrected using a Mark-Houwink relation to take account for the different hydrodynamic radii of polystyrene and the AN-co-MA-polymers[24] (see Figure SI11), and the average degrees of polymerization P_n were found to be in the range between 180 and 230. All samples of this study showed a monomodal distribution with a dispersity M_w/M_n ($Đ$) of about 2. The average degree of polymerization P_n can also be determined by means of ^{1}H NMR spectroscopy via end group analysis using the signals of the two inequivalent methyl groups of the isobutyronitrile end group originating from the azoisobutyronitrile initiator (AIBN) which appear at 1.37 and 1.41 ppm in DMSO-d^{6} versus the broad signal for the CH_2 groups of the backbone in the range between 1.6 and 2.3 ppm (Figure 4). For this evaluation it must be taken into account that the termination step during radical polymerization of AN is by far dominated through recombination rather than disproportion (as evidenced by the lack of olefinic signals in the ^{1}H NMR spectrum found for all samples of this study; for $Đ$ in this case a value of 1.5 rather than 2 would have been expected. However, the accuracy of $Đ$ from the SEC measurements is not high enough to distinguish these two cases confidently). Thus, the isobutyronitrile methyl end groups at

1.37 and 1.41 ppm account for 12 H atoms per macromolecule (not 6!) relative to the 2 H atoms per CH_2 backbone repeat unit in the macromolecule. The results are in acceptable agreement with the SEC data. Still, because of the broadness of the peaks we recommend to use the ^{1}H NMR evaluation only as a double-check of the SEC results and not as a reference. The accuracy of the ^{1}H NMR results is, according to our evaluation, at best ±15%.

The degree of crystallinity of the polymeric samples was determined by means of X-ray powder diffraction (XRD). The evaluation of the diffractograms was done using the peak at $2\theta = 16.9°$ according to the method of Bell and Dumbleton which might slightly underestimate the degree of crystallinity.[25,26] For all our samples we received crystallinity indices of about 50 ± 5% (see Figure SI12). The degree of crystallinity is important for the thermal treatment, because there exists evidence that the transformations take place at first in the amorphous regions of the material and only retarded in the crystalline domains.[27]

2.2 | Characterization devices

2.2.1 | Simultaneous thermal analysis

TGA and optionally differential thermal analysis (DTA) or differential scanning calorimetry (DSC) were performed simultaneously using the simultaneous thermal analysis (STA) 449 F3 Jupiter (Fa. NETZSCH-Gerätebau GmbH). The TG-DTA sample carrier with 0.3 ml Al_2O_3 crucibles was used to heat the PAN copolymer powder samples with a rate of 10 K/min up to 420°C under inert atmosphere of Helium (70 ml/min). Initial sample weights between 25 and 55 mg were used in this setup to acquire thermogravimetric signals with a resolution of 1 µg and DTA data showing signatures of thermal events with sufficient quality. Quantitative results of reaction enthalpies were obtained by the STA with a TG-DSC sample carrier. STA-Data were analyzed using the software NETZSCH Proteus version 6.1.0.

Evolved gas analysis was performed using the "Perseus" coupling of the FTIR spectrometer ALPHA (Fa. BRUKER Optik GmbH) mounted directly onto the gas outlet of the STA furnace. An additional outlet of this connection allowed for the simultaneous coupling to a gas chromatograph (7890A) with a mass spectrometer detection system (VL MSD 5975C, Fa. Agilent Technologies; software: MSD ChemStation E.02.02.1431). The GC system with a HP5MS column was modified by a valve box for automated injection of the 250 µl sample loop content (cycle time: 2 min; Fa. Joint Analytical Systems—JAS GmbH). To prevent condensation of volatiles all coupling connections were heated to at least 220°C, the gas cell of the FTIR spectrometer to its specified maximum temperature of 200°C.

FTIR absorbance spectra were recorded continuously approximately every 12 s with a resolution of 4 cm^{-1} between wavenumbers of 550 and 4400 cm^{-1}. An additional dinitrogen purge gas flow through the IR mirror parts of the spectrometer was used to keep the background signal constant during the time of the measurement runs, especially to avoid varying water and carbon dioxide contaminations in the optical path of the IR beam before and after passing the KBr windows of the gas cell. An additional silylated stainless steel tube of 2 mm inner diameter (SilcoNert 2000, Fa. Silcotek GmbH) was temporarily mounted inside the transfer line at the inlet of the FTIR gas cell ending about 2 cm above the sample position. This inerted snorkel allowed for reduced H/D exchange effects of the evolved deuterated gas species with the tube surface at least between the sample crucible and the entrance of the gas cell.

Data acquisition and export was done with the software OPUS 7.0 (Fa. BRUKER Optik GmbH).

Separation of the experimental FTIR spectra into specific target compounds was achieved by consecutive subtraction of reference spectra for each target compound (measured separately and weighted by a linear coefficient) from the experimental spectrum to take account as good as possible for the total intensity found, where the order of subtraction is decisive and had to be carefully worked out (see Figure SI14). Characteristic bands for each target compound with minimum overlap to bands of other evolved gas species during PAN copolymer decomposition were identified on this purpose.

Quantitative evaluation of the FTIR data required preceding calibration measurements with the pure species (H_2O, D_2O, CH_3OH, CD_3OH, CH_3OD, and CD_3OD) or decomposing solid samples evolving the target compounds in defined stoichiometric amount ($(NH_4)HCO_3$, $(NH_4)CH_3COO$, Ag_2CO_3, $Ag_2{}^{13}CO_3$, $(NH_4)_2Fe(CN)_6$, $(ND_4)_2Fe(CN)_6$, and $Zn(^{15}NH_3)_2Cl_2$) and determination of the calibration factor between absorbance intensities of characteristic absorption bands in the FTIR spectra and mass loss rates in the STA. As absorbance signal intensities can show non-linear behavior with respect to the concentration (Beer–Lambert law), this calibration factor had to be determined as function of different mass loss rates, covering the relevant range of evolved gas concentrations occurring during the subsequent PAN copolymer sample measurements (see Figure SI13–16).

2.2.2 | In-situ Fourier transform infrared spectroscopy

All powders were distributed in CsI-pellets to prepare them for the IR measurement. The proportion was 40 mg of CsI-powder to 1 mg of PAN-powder.

A small furnace was used to heat up the sample with a constant rate of 5 K/min. Temperatures between room temperature and 420°C were realized. The furnace was placed within an FTIR spectrometer (ALPHA (Fa. BRUKER Optik GmbH)). During the heating, simultaneously IR-spectra were recorded in transmission with a rate of about 2.5 spectra/min. The range of wave numbers was from 1000 to 4500 cm^{-1} with a resolution of 2 cm^{-1}. The setup was kept under dinitrogen atmosphere.

2.2.3 | Solid-state NMR spectroscopy

Solid State magic angle spinning (MAS) NMR experiments for samples P9 and P17 were performed on a Varian VNMRs 500 spectrometer operating at 11.7 T. A 1.6 mm T3 MAS NMR probe was used for all experiments. For the ^{2}H single pulse acquisition measurements and ^{2}H-{^{1}H} and ^{13}C-{^{1}H} CPMAS NMR measurements recycle delays of 20–50 and 10–20 s were used with typical spinning speeds of 25 kHz and 6–10 kHz, respectively. ^{13}C and ^{15}N single pulse acquisition MAS NMR spectra were recorded at spinning frequencies of 12 kHz and recycle delays of 200 s to obtain quantitative spectra.

^{13}C-{^{15}N} rotational echo double resonance (REDOR) NMR experiments were performed employing spinning frequencies of 8–16 kHz and recycle delays of 10–20 s. Typical π-pulse lengths of 5.25 μs for ^{13}C and 9 μs for ^{15}N were used. Spectra were simulated using the SIMPSON[28] software. To facilitate acquisition of NMR spectra, the magnetization of carbon nuclei was prepared via cross polarization (CP) from ^{1}H. For the ^{15}N-{^{1}H} CPMAS heteronuclear correlation (HETCOR) and ^{13}C-{^{15}N}-{^{1}H} double CPMAS HETCOR experiments recycle delays of 5–20 s were used. For the latter, an initial $^{1}H \rightarrow {}^{15}N$ cross polarization step (contact time 6 ms) was followed by a $^{15}N \rightarrow {}^{13}C$ cross polarization step (contact time 0.5 ms).

^{13}C-{^{1}H} and ^{15}N-{^{1}H} CPMAS of sample P18 were performed on a Bruker Advance III 300 MHz spectrometer operating at 7.05 T and employing a 4 mm MAS probe. Recycle delays of 10–20 s and typical spinning speeds of 6–10 kHz were used.

In all measurements chemical shifts were referenced to adamantane ($\delta(CH_2) = 38.5$ ppm for ^{13}C and $\delta(CH_2) = 1.75$ ppm for ^{1}H), glycine ($\delta[N] = -346.8$ ppm) for ^{15}N and acetone-d^6 (2.0 ppm for ^{2}H).

2.2.4 | Characterization devices and settings used for the monomers, model compounds and starting copolymers

The IR measurements were performed using a Thermo Nicolet FT/IR machine (Fa. Nexus) in the ATR mode (diamond crystal) at room temperature and were evaluated using the software package OMNIC 6.1a.

The solution NMR data were collected using a Mercury plus400 high resolution console (Varian/Agilent) with a PFG ATB broadband probe (1H/19F/X 5 mm) and were evaluated using the software package VNMR 2.2a. The NMR measurements of the monomers and model compounds were done using $CDCl_3$ as solvent (7.26 ppm in ^{1}H, 77.0 ppm in ^{13}C; ^{15}N chemical shifts are given relative to nitromethane = 0 ppm). For the copolymer samples, DMSO-d^6 was used as solvent (2.49 ppm in ^{1}H, 39.5 ppm in ^{13}C).

The elemental analysis was done on a VARIO EL III CHNS device (Fa. Elementar Analysensysteme GmbH).

A Guinier-type powder X-ray diffractometer equipped with a G670 imaging plate detector (Fa. Huber) and Cu-$K_{\alpha 1}$ radiation was used for the determination of the crystallinity index. Samples were placed between two sheets of 6 μm thick PET foil and data were collected in transmission mode. The background contribution of the foil was carefully subtracted using a reference measurement without sample.

Suitable single crystals of compounds **A**, **B**, and **P^{200}** were mounted onto a Dual Thickness MicroLoop LD (Fa. MiTeGen) using small amounts of perfluoropolyalkylether (viscosity 1800 cSt., Fa. ABCR). Data were collected on a SMART-APEX diffractometer equipped with a D8 goniometer and an APEX II CCD detector (Fa. Bruker), a microfocus X-ray tube with Ag-K_{α} radiation and Helios mirror optics (Fa. Incoatec). During data collection, the crystals were kept at a temperature of 100(2) K using a Cryostream 700 low temperature device (Fa. Oxford Cryosystems).

CCDC 2023177, 2023179 and 1825233 contain the supplementary crystallographic data for compounds **A**, **B**, and **P^{200}** of this paper. These data can be obtained free of charge from The Cambridge Crystallographic Data Centre via www.ccdc.cam.ac.uk/structures.

2.2.5 | Size exclusion chromatography

The SEC system was equipped with a SpectraSYSTEM P1000 pump set to a nominal flow rate of 0.7 ml/min, a SpectraSYSTEM AS1000 autosampler and a LaChrom RI-Detector L-7490. Separation was performed on a MZ-Gel SDplus linear column (5 μm, 300 × 8 mm) and two MZ-Gel SDplus guard columns (50 Å, 100 Å, 50 × 8 mm each).

HPLC-grade DMF, containing 0.01 mol/L LiBr was used as mobile phase. The experiments were performed at 60°C. The evaluation was done using a polystyrene standard and was corrected via Mark/Houwink relation.[24]

2.2.6 | Micro sieve tower

A micro sieve tower (Fa. Linker Industrie-Technik) with five mesh sizes (50, 100, 250, 500, and 1000 μm), diameter for each size container 50 × 25 mm was used to separate the polymer powder into fractions of different particle size.

3 | RESULTS AND DISCUSSION

3.1 | Differential scanning calorimetry/thermogravimetric analysis results of the polymeric samples

Figure 5 shows the dependence of the DSC and TGA results on the MA content. The results have been collected under inert He atmosphere at a heating rate of 10 K/min.

While the onset temperature is comparable in all cases at about 265°C, the maximum of the thermal signature shifts to higher temperatures with increasing MA content and the complete peak broadens over a larger temperature range, demonstrating a retarding effect of MA on the stabilization process. We will give a convincing explanation for this behavior in this paper. At MA contents larger than about 6% a shoulder is observable on the left hand side of the thermal peak. These results are independent of the mesh size of the polymeric powder. A change in the heating rate does not lead to a clearer separation of the observed shoulder. The weight loss in particular during the main heat release is reduced with increasing MA content.

3.2 | Evaluation of the volatiles stemming from the methyl acrylate moiety (simultaneous thermal analysis)

Even during the thermal treatment of PAN homopolymer under inert atmosphere a plethora of volatile compounds are formed (left hand side part of Figure 6), and in a recent paper we have described how we can qualitatively and in parts quantitatively determine them via EGA by means of FTIR spectroscopy and GC/MS determination coupled to STA. We also have proposed mechanisms for their formation.[21] EGA has again been applied in this study and since both characterization methods involved are sensitive to isotopic changes, with our collection of selectively isotopically labeled copolymer samples we are in the position to challenge, sharpen and extend the existing mechanistic considerations. In this publication, we focus on the volatiles connected with and related to the comonomer MA (right hand side part of Figure 6). A similar analysis concerning the volatiles related to AN has been performed by us, but it would overload this publication to present everything in one paper. Nevertheless, we can already state that our findings support the principle mechanisms including a Ziegler-Thorpe reaction followed by a retro-hetero-en reaction and a Hantzsch-type reduction as a main reaction pathway for the formation of most of these volatiles stemming from AN subunits.

Volatile compounds that obviously must stem from the MA comonomer are those containing oxygen. Beside of carbon dioxide and water, methanol (surprisingly, to the best of our knowledge for the first time; methanol formation by reaction of the MA repeat unit with ammonia has been briefly mentioned in Reference [14] however for the special case of applying an ammonia atmosphere during the thermal treatment) is the third of these compounds unequivocally detected by FTIR spectroscopy. Figure 7 illustrates the development with temperature of these three volatiles along with ammonia and HCN in the STA treatment of sample P6 determined via FTIR spectroscopy. The non-trivial quantitative evaluation of the complex IR spectra found during the EGA measurement via a deconvolution method using the consecutive subtraction of reference spectra of the pure compounds

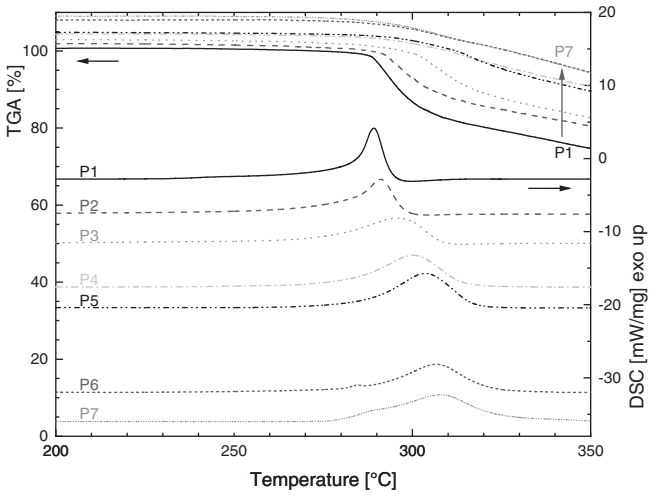

FIGURE 5 Differential scanning calorimetry thermograms (bottom) and thermogravimetric analysis results (top) of selected samples with increasing methyl acrylate (MA) content from sample P1 to P7 (heating rate: 10 K/min). Vertical shift of waterfall plot curves scaled by the MA content

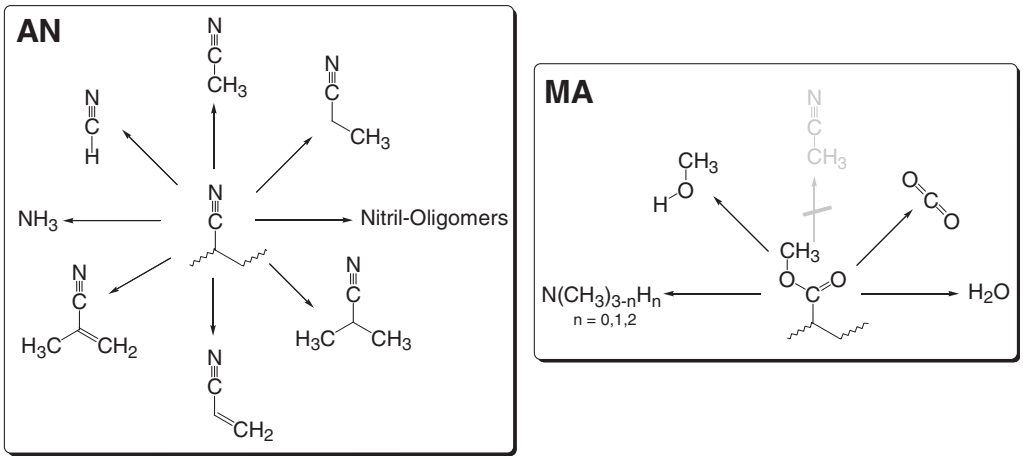

FIGURE 6 Important volatiles formed during the thermal treatment of acrylonitrile (AN)-co-methyl acrylate (MA) co-polymers related to the AN repeat unit (left) and related to the MA repeat unit (right)

from the net spectrum weighted by carefully determined calibration factors is described briefly in the Figures SI13 and SI14. Ammonia and HCN (which themselves of course are not formed from MA) are added into the figure because as we will show below both (and in particular ammonia) play a crucial role in the discussion of formation mechanisms of the volatiles related to MA.

Interestingly, volatile methyl ester compounds analogous to the oligomeric volatile nitriles shown in Figure 6 such as methyl acetate, methyl propionate, methyl acrylate and methyl methacrylate were not found during the thermal treatment of the AN-co-MA polymers.

3.2.1 | Methanol

The first volatile that can be detected by means of FTIR spectroscopy in the course of the thermal transformation of the AN-co-MA polymers is methanol. It came as a surprise to us that this compound has not been mentioned in prior publications to the best of our knowledge. The onset of the methanol formation is found to be independent of the MA content at about 245°C under the conditions applied (heating rate 10 K/min). The maximum of methanol formation precedes the DTA signal maximum by about 9°C independent of the MA content, while the shapes of the two signals (DTA signal and FTIR-trace) are the same, and it shifts to higher temperatures with increasing MA content. The formation of methanol is limited to this early stage of the thermal transformation and is completely finished below temperatures of about 325°C (Figures 7 and 8). The amount of formed methanol as function of MA content is shown in Figure 9 using the data of Table 2.

The yield Y^{MeOH} relative to the MA content can be calculated quite confidently by the empirical formula

$$Y^{MeOH} \approx 1.45 \times x(MA)^{0.33} \times [1 - x(MA)]^3, \qquad (1)$$

where x(MA) is the content of MA in the material. This yield is independent of the mesh size of the polymeric powder (tested for mesh sizes <50, 50–100, 100–250 and 250–500 μm).

Although the above-mentioned formula is just empirical and we cannot give a theoretical derivation for it, it qualitatively represents what we expect for the methanol yield over the complete range of MA content (Figure 10).

In particular, we do not expect a saturation value for the methanol yield at high MA content (for example a sample of PMA homopolymer treated under the same conditions as the AN-co-MA polymers did not show a methanol formation in the temperature regime below 350°C with a methanol yield of about 22% [formation maximum above 400°C]).

According to the reaction pathways that we will suggest below the formation of methanol requires ammonia (formed from the AN units), as a stoichiometric reagent (e.g., amidation reaction) or/and as a catalyst (e.g., Diekmann-analogous reaction).

In range **A** of Figure 10 ammonia is formed in high amounts, however the MA units are too diluted along the chain to be reached by the ammonia prior to its evaporation. This limits the methanol formation.

In range **B** of Figure 10 ammonia is formed in still high enough amounts, and the MA units are concentrated enough along the chain now to be reached by the ammonia prior to evaporation. More methanol is formed.

In range **C** of Figure 10 ammonia is formed in smaller amounts and becomes limiting, even though the MA

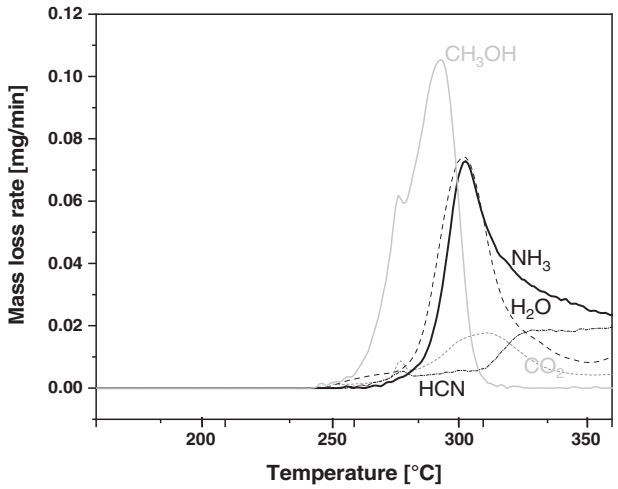

FIGURE 7 Fourier transform infrared-traces of methanol, carbon dioxide, water, ammonia and HCN as found in the thermal treatment of sample P6 (heating rate: 10 K/min; thermal differential scanning calorimetry peak maximum at 302°C)

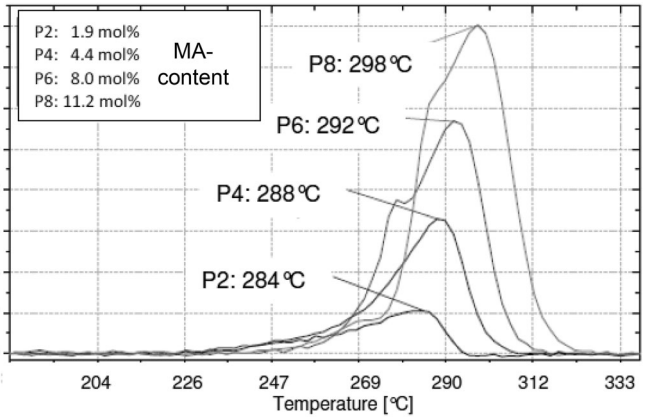

FIGURE 8 Fourier transform infrared-traces of methanol for samples with different methyl acrylate content (heating rate: 10 K/min)

units are concentrated enough along the chain to be reached by the ammonia prior to evaporation. This leads to a decrease in methanol formation.

To support this explanation, two additional samples have been examined that are not mentioned in Tables 1 and 2 because the MA contents are out of the technically relevant range (16 mol% d^1-MA and 19 mol% d^2-MA).

Thus, according to our proposal the formation process of methanol is at least dominated by the kinetic counterplay between the time interval during which formed ammonia remains bound to the polymeric material via hydrogen bonding (enabling the amidation/amidination reaction) and ammonia loss to the gas phase.

With about 45%–53%, the pathways releasing methanol account for about half of the amount of thermal transformations concerning all MA units in the range of 5–10 mol% MA content.

For sure the complete formation mechanism of methanol is complex, but still we want to mention (although without further concluding important aspects from it) that a comparison of the yields for our non-labeled copolymers with those for the deuterated ones point towards isotopic effects in some cases. For d^1-AN a normal and for d^1-MA an inverse small isotopic effect is observed (for P15 with both labelings in one material the found normal isotopic effect of d^1-AN is decreased as would have been expected). For d^3-MA also a normal isotopic effect is observed, which was unexpected. For d^2-AN a normal isotopic effect is found, while d^2-MA does not show any significant deviation from the methanol yield received with the non-labeled materials.

Taking the results of Figure 7 that the methanol formation precedes the detection of released ammonia by means of FTIR spectroscopy while the thermal fingerprint measured by means of DTA parallels the release of ammonia, we conclude that the formation of methanol is connected with the consumption of formed ammonia which itself is lost for the anticipated stabilization processes which are mainly responsible for the thermal fingerprint, and this is the reason why with increasing MA content in the material the thermal transformation shifts to higher temperatures. We will give proposals for concrete chemical reaction pathways below.

In view of these results we have further examined the role of ammonia for the formation of methanol.

As can be seen in Figure 11 (top) in the samples containing AAM the formation of ammonia (along with the thermal stabilization processes) is shifted to decisively lower temperatures (compare P18 with P6 in Figure 11) since the amide groups with their mobile hydrogens act as initiators for the cyclization reaction (a fact that is already generally agreed on).

Three samples have been examined to gain a deeper insight into this process:

1. a physically mixed sample of P6 and P18 (prepared by grinding equal amounts). In this sample the early formed ammonia of P18 is in a different phase than the MA contained in P6 (Figure 11; third from top).
2. a blended chemically mixed sample of P6 and P18 (prepared by dissolving equal amounts in DMF and precipitating them with excess methanol and drying in vacuo). In this sample the early formed ammonia of P18 is in the same phase as the MA contained in P6, however it is not formed in the same macromolecule (Figure 11; second from bottom).

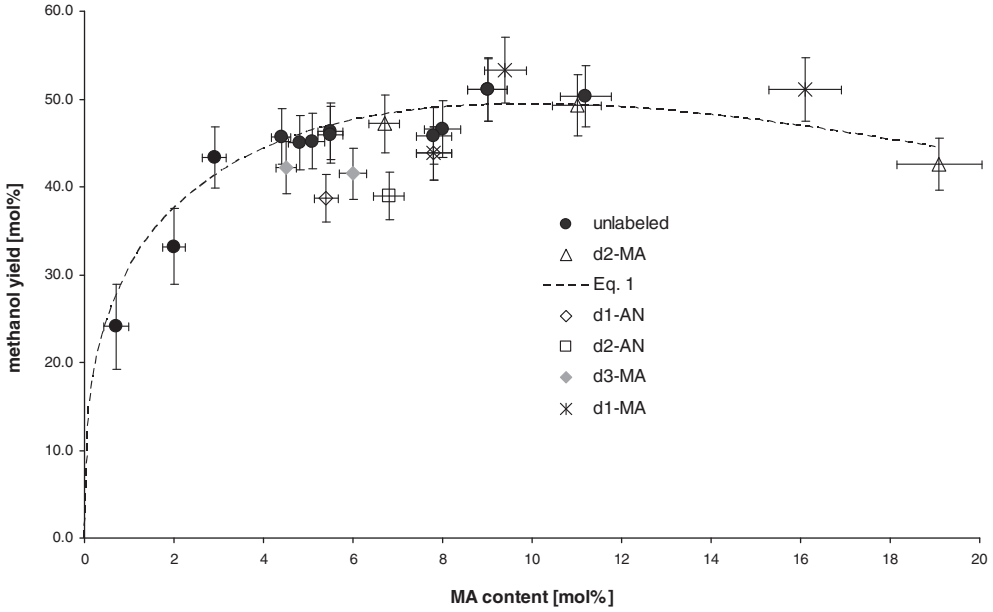

FIGURE 9 Yield of formed methanol as function of methyl acrylate (MA) content (two additional samples at irrelevant high MA content for the technical application are included to support our conclusions and proposals mentioned in the text; heating rate: 10 K/min)

TABLE 2 Total methanol yield of the different samples (heating rate: 10 K/min)

Sample	Labeling	MA content (mol%)	Methanol yield[a] (mol%)
P1	–	0.7 ± 0.04	24 ± 5
P2	–	1.9 ± 0.1	33 ± 5
P3	–	2.9 ± 0.1	43 ± 4
P4	–	4.4 ± 0.2	46 ± 4
P5	–	5.1 ± 0.3	45 ± 4
P6	–	8.0 ± 0.4	47 ± 4
P7	–	9.0 ± 0.5	51 ± 4
P8	–	11.2 ± 0.6	50 ± 4
P9	CD_3-MA	4.5 ± 0.2	42 ± 4
P10	d^1-AN	5.4 ± 0.3	39 ± 4
P11	d^2-AN	6.8 ± 0.3	39 ± 4
P12	d^1-MA	9.4 ± 0.5	53 ± 5
P13	d^2-MA	11.0 ± 0.6	49 ± 4
P14	d^2-MA	6.7 ± 0.3	47 ± 4
P15	d^1-AN, d^1-MA	7.8 ± 0.4	44 ± 4
P16	^{15}N-AN, CD_3-MA	6.0 ± 0.3	41 ± 4
P17	^{15}N-AN, ^{13}CO-MA	10.1 ± 0.7	41 ± 4

[a]Sum over all isotopomers found; yield relative to MA content.

3. the copolymerized sample P19 (AN-co-MA-co-AAM). In this sample the early formed ammonia is present in the same phase and even formed in the same macromolecule as the MA moiety (Figure 11; bottom).

We note that an early formation of methanol in considerable amounts is only observed in samples (b) and (c) (and by far mainly in c)). We also note that the total amount of detected methanol in sample a.) (total MA content: 8.0/2 = 4 mol%), is comparable to that found for samples P6 (MA content: 8.0 mol%) and P19 (MA content: 6.9 mol%), while for sample b.) (total MA content: 8.0/2 = 4 mol%) the total amount of detected methanol is decisively smaller, supporting the following important aspects:

1. The formation of methanol is related to and connected with ammonia.

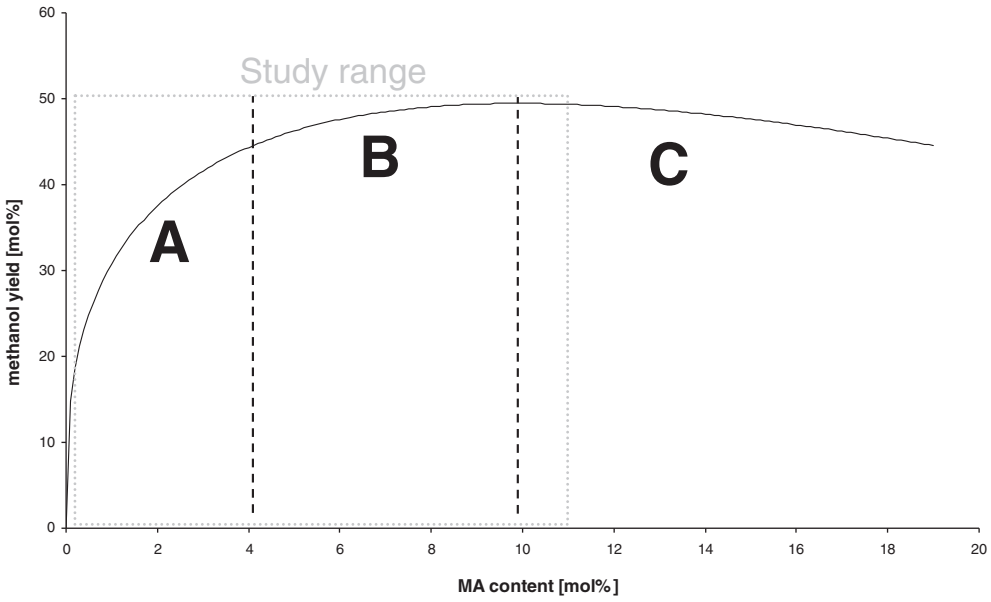

FIGURE 10 Expected development of formed methanol as function of methyl acrylate (MA) content. The ranges A, B and C are explained in the text

2. In sample a.) the two grinded polymers behave evidently mainly as two independent phases according to the total amount of formed methanol, in contrast to the blended sample b.) taking the decisively smaller total amount of formed methanol.
3. Thus, as a conclusion the required ammonia is conducted to the reaction centers mainly (but not exclusively) intramolecularly along the macromolecule at which it is generated, as we propose via maintaining hydrogen bonding between the macromolecule and the ammonia (chemical mechanisms will be shown below in the conclusion; the formation of methanol in sample c) via cyclization reaction initiated by the amide groups also requires ammonia as catalyst according to our proposal (Figure 30)).

A further question to be addressed with our powerful set of selectively labeled samples (in particular the deuterated ones P9−P16) is how the methanol is formed. We will first present our experimental results. In the conclusion below we will propose detailed chemical reaction pathways based on these results.

Concerning the samples P9−P16 the three differently deuterated isotopomers CH_3OH, CH_3OD and CD_3OH can be formed, providing the possibility to give insight into where the hydrogens of the evolving methanol stem from in the original material.

These three isotopomers can be distinguished and even be quantified via FTIR spectroscopy using our deconvolution method (see Figure SI13). The relative amounts of isotopomers found (not the yields relative to the MA content, which are shown in Table 2) are listed in Table 3.

From samples P9 and P16 we can unequivocally prove that all methanol evolving during the thermal treatment of the polymeric powders originates from the MA methoxy moiety (excluding among others methanol used for the washing process of the polymeric powder starting material). The three hydrogens of the methanol methyl group stem from this and only from this moiety. d^3-Methanol is the least problematic deuterated compound for unequivocal conclusions, because H/D scrambling effects with polar X—H moieties of other compounds in the gas phase, other functionalities in the solid residual or with the STA device walls can be ruled out for it. For d^1-methanol, ammonia and water, which are discussed next, such kinds of H/D scrambling effects must be considered, since they might at least partly distort an unequivocal chemical correlation between the origin of a deuterium labeling (which is defined) and the detection of it in one of these volatile compounds.

Concerning the H/D scrambling with the device walls we temporarily implemented a silylated snorkel into our commercial STA device inside the transfer line at the inlet of the FTIR gas cell ending about 2 cm above the sample position. This significantly increased the amount of found d^1-methanol as well as deuterated ammonia and deuterated water isotopomers proving that an H/D scrambling with the device walls is substantially active. Thus, all quantitative values for d^1-methanol and deuterated water isotopomers must be considered as a lower limit of the real value (for the ammonia isotopomers only qualitative values are given as will be explained below).

Concerning the H/D scrambling between the three volatile compounds in the gas phase which would at least partly level out a conclusive mechanistic relation between origin and final position of the deuterium

labeling, we notice that regarding the degree of deuteration for methanol, ammonia and water the same principle tendencies are found over all samples of this study

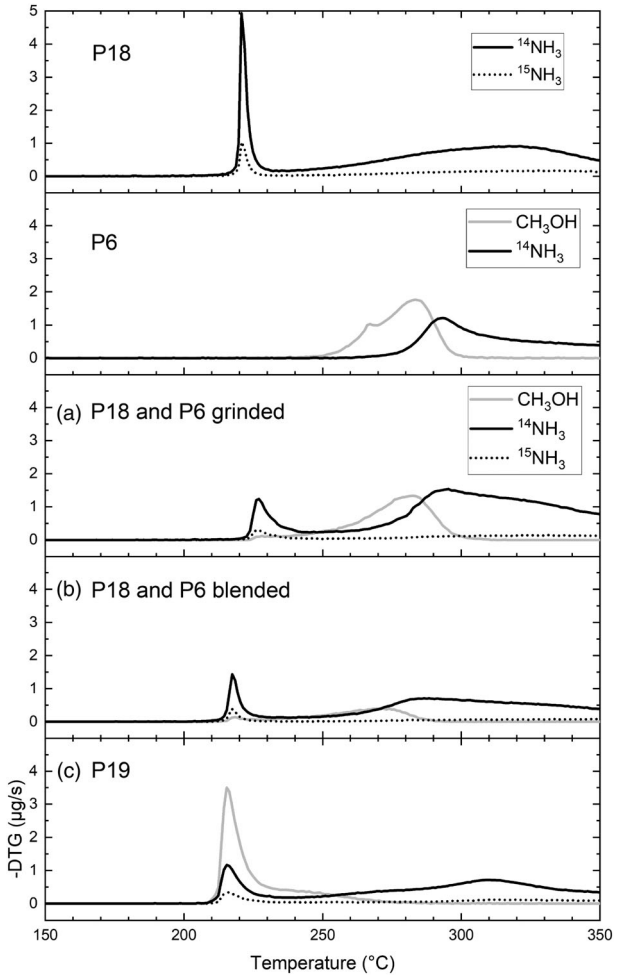

FIGURE 11 Mass loss rates of ammonia and (if present) methanol in P18 and P6 as function of the temperature compared to the three samples (a), (b) and (c) described in the text during the evolved gas analysis measurement (for the determination of $^{14}NH_3/^{15}NH_3$ isotopomers by means of Fourier transform infrared spectroscopy see also Reference [21]; heating rate: 5 K/min)

(Tables 3, 4 and 5), and in the first place this is a situation where a possible partial equilibration by H/D scrambling between the compounds cannot be distinguished unequivocally from consecutive chemical correlations concerning the formations of these compounds. However, a re-inspection of Figure 7 focusing on the order in which the compounds are formed in time reveals some reason for hope. In particular by far most of the methanol is detected decisively before water and ammonia, and, thus, by far the majority of methanol is not present in the gas phase simultaneously with any other volatile compound rendering an H/D scrambling impossible. For water and ammonia, which are evolving approximately simultaneously (water a little before ammonia), a simple H/D scrambling in the gas phase between them cannot be cleared out unequivocally, unfortunately.

The same dilemma is true concerning a possible H/D scrambling between the volatile compounds and the residual solid since also for the degree of deuteration within the residual solid the principle tendencies parallel those of methanol, ammonia and water (see Figure 13).

However, since according to our assessment and also to our already presented experimental results it is strongly reasonable to take into account an existing consecutive chemical correlation in the formation process (bulk material → ammonia → methanol) and (bulk material → ammonia → water), we still present individual data for all isotopomers (Tables 3, 4 and 5) wherever it is possible for us and, with due caution, we will propose consecutive chemical formation mechanisms that are in accordance with our experimental data, although honestly we must state that they do not prove the mechanisms in last instance because of the ambiguity connected with a possible H/D scrambling. In addition, this should be kept in mind of the reader.

An interesting general finding regardless of the H/D scrambling problem is doubtless that for samples P11 and

TABLE 3 Relative amounts of different methanol isotopomers found by means of Fourier transform infrared spectroscopy (heating rate: 10 K/min)

Sample	Label	CH_3OH (%)	CH_3OD (%)	CD_3OH (%)
P9	CD_3-MA	0	0	100
P10[a]	d^1-AN	32	68	0
P11[a]	d^2-AN	81	19	0
P12[a]	d^1-MA	85	15	0
P13[a]	d^2-MA	>98	<2	0
P14[a]	d^2-MA	>99	<1	0
P15[a]	d^1-AN, d^1-MA	46	54	0
P16	^{15}N-AAM, CD_3-MA	0	0	100

[a]Measurement with implemented inerted snorkel in the simultaneous thermal analysis device.

P12 significant amounts of deuterium are found in all volatile products in the focus of this study.

3.2.2 | Ammonia

The maximum of ammonia formation is almost identical with that of the thermal signal. We point out that volatile ammonia starts to be detected not before the amount of formed methanol begins to cease (Figure 7). Since our results suggest that the formation of methanol is connected and correlated with a consumption of ammonia this raises the question about the degree of deuteration in ammonia, which translates into a specific deuteration in methanol via catalytic pathways or stoichiometric reactions. All four isotopomers $NH_{3-n}D_n$ ($n = 0, 1, 2, 3$) can be resolved and distinguished by means of FTIR spectroscopy (Figure 12). However, only for NH_3 we were able to determine a confident calibration factor to quantify its amount. Still qualitatively the relative amounts of the isotopomers can be compared assuming that the oscillation strength of the vibrations does not differ dramatically from isotopomer to isotopomer.

In contrast to methanol the formation of ammonia continues to a considerable amount even after the thermal main peak has ceased. Table 4 lists the qualitative relative amounts of ammonia isotopomers found within the main thermal peak at temperatures between 270 and 330°C. The found ammonia isotopomers with different deuteration degree parallel those of methanol and water including the problem of H/D scrambling mentioned above (in particular between water and ammonia).

TABLE 4 Relative amounts of different ammonia isotopomers found by means of Fourier transform infrared spectroscopy

Sample	Label	Released ammonia isotopomers
P9	CD_3	**NH_3** exclusively
P10[a]	d^1-AN	**ND_3** ≈ **ND_2H** > NDH_2 > > NH_3
P11[a]	d^2-AN	**NH_3** > > NH_2D > ND_2H > ND_3
P12[a]	d^1-MA	**NH_3** > > NH_2D > NHD_2 > > ND_3
P13[a]	d^2-MA	**NH_3** exclusively
P14[a]	d^2-MA	**NH_3** exclusively
P15[a]	d^1-AN, d^1-MA	**ND_3** > **ND_2H** > > NDH_2 > NH_3

[a]Measurement with implemented inerted snorkel in the simultaneous thermal analysis device.

TABLE 5 Relative amounts of different water isotopomers found by means of Fourier transform infrared spectroscopy (heating rate: 10 K/min)

Sample	Label	Relative water isotopomer yields (%)		
		H_2O	**DHO**	**D_2O**
P9	–	100	0	0
P10[a]	d^1-AN	4	41	55
P11[a]	d^2-AN	56.5	35	8.5
P12[a]	d^1-MA	79	20	1
P13[a]	d^2-MA	>97	<2	<1
P14[a]	d^2-MA	>98	<1	<1
P15[a]	d^1-AN, d^1-MA	17	40	43

[a]Measurement with implemented inerted snorkel in the simultaneous thermal analysis device.

3.2.3 | Water

With about 40%–60% yield relative to the MA content (at MA contents between 5 and 10 mol% in the starting material) water is detected in molar amounts comparable to methanol by FTIR spectroscopy. We were able to determine calibration factors for all three isotopomers, a task that is everything but trivial, and could, thus, quantify the formed amounts of them (Table 5; concerning the evaluation see Figure SI15). Concerning the three isotopomers the same tendencies as for methanol and ammonia are found in dependence on the selective deuteration in the starting material. The formation of water is not as completely finished as that of methanol within the main thermal peak. We mention that an H/D scrambling between water and ammonia in the gas phase might distort conclusions about chemical reaction mechanisms (although again: a lot of

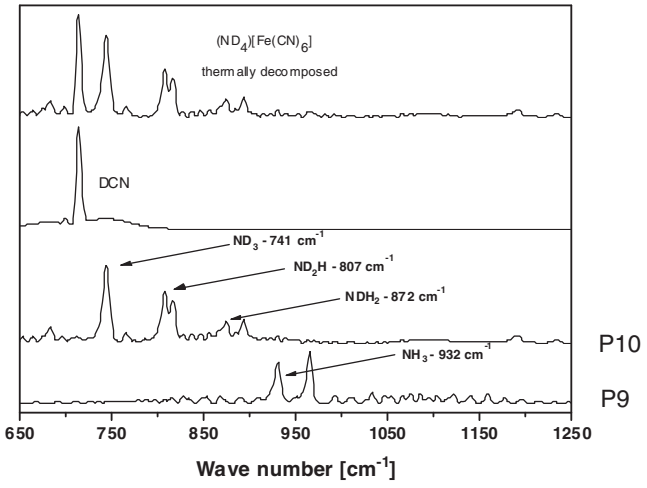

FIGURE 12 Fourier transform infrared spectra containing the four different ammonia isotopomers in comparison

results speak in favor of consecutive chemical correlations as the reason for the similar degrees of deuteration in the different examined compounds and moieties).

3.2.4 | Carbon dioxide

$^{13}CO_2$ can unequivocally be distinguished from $^{12}CO_2$ in the FTIR spectrum by its isotopic shift and we were able to determine calibration factors for the quantification of both isotopomers (Table 6; see Figure SI16). Interestingly, on examination of sample P17 we did not only find $^{13}CO_2$ but also a considerable amount of $^{12}CO_2$ (both evolving time-parallel to each other). The sum of found CO_2 over both isotopomers in P17 equals approximately that found for the samples without labeling (Table 6). Thus, concerning the formation mechanism of CO_2 we must consider that while most of the formed CO_2 stems directly from the original MA moiety position, a considerable amount is formed elsewhere using other carbon atoms than the MA carbonyl carbon.

3.2.5 | Concluding remarks concerning the three main volatiles formed from MA (MeOH, H_2O, and CO_2)

In a first conclusion concerning the volatile compounds methanol, ammonia, water and carbon dioxide we state:

1. The formation of methanol is correlated to the formation of ammonia.
2. At least along one pathway ammonia is consumed during the formation of methanol.
3. As long as ammonia is consumed by the generation of methanol the thermal cyclization reaction is hampered. This is the reason why the thermal signal is shifted to higher temperatures by about 9 K relative to the methanol formation and that the thermal transformation of the AN-co-MA-polymer with increasing amount of MA is shifted to higher temperatures while always the formation of ammonia parallels the thermal signal.
4. The ammonia molecules are conducted to the reaction center mainly (but not exclusively) intramolecularly along the macromolecule at which they are formed, as we propose via maintaining hydrogen bonding between the ammonia and the nitrogen moieties of the macromolecule.
5. All methanol is formed from the MA methoxy group.
6. Most CO_2 but by no means all is formed directly from an original MA moiety.

Assuming that H/D scrambling in the gas phase and in the bulk material can be neglected (with due caution):

1. Since the tendencies in the degree of deuteration is similar in all samples for ammonia, methanol and water, this is in accordance with a consecutive formation process and, thus, a chemical deuterium transfer from one moiety to the other.
2. The transferred hydrogens in this possible consecutive chemical formation process stem mostly from the methine position of the polymer and preferably from MA methine groups over AN methine groups; however, a significant minor amount also stems from the methylene groups (in this case the methylene group of the AN repeat unit is preferred over the methylene group of the MA repeat unit).

Proposals for detailed chemical reaction mechanisms explaining these conclusions are given in the conclusion section below.

3.2.6 | Methyl amines and acetonitrile

Two volatile compounds that are not obvious in the first place to be brought into connection with the MA moiety

TABLE 6 Exemplary yields of CO_2 isotopomers found by means of Fourier transform infrared spectroscopy (heating rate: 10 K/min)

Sample	Labeling	MA (mol%)	$^{12}CO_2$ yield (mol%)	$^{13}CO_2$ yield (mol%)
P5	–	5.1 ± 0.3	8.9 ± 0.9	0
P6	–	8.0 ± 0.4	9.5 ± 0.9	0
P17	^{15}N-AN, ^{13}CO-MA	10.1 ± 0.7	4.5 ± 0.5	7.8 ± 0.8
P10	d^1-AN	5.4 ± 0.3	9.6 ± 0.9	0
P11	d^2-AN	6.8 ± 0.3	11.4 ± 1.1	0
P12	d^1-MA	9.4 ± 0.5	11.6 ± 1.1	0
P13	d^2-MA	11.0 ± 0.6	10.1 ± 1.0	0

are methyl amines (mono-methylamine, dimethyl amine and trimethyl amine) and acetonitrile. In fact, whether these compounds are connected with the MA unit, can only be proven by inspection of samples P9 and P16 with perdeuterated methyl groups in the MA moiety. In these samples acetonitrile and the methyl amines should be found with perdeuterated methyl groups.

In the case of acetonitrile the situation is complicated by the fact that even during the thermal transformation of simple PAN homopolymer (without MA units) acetonitrile is formed and observed. We have carefully examined the volatile fraction of samples P9 and P16 by means of GC/MS, and we could not find perdeuterated acetonitrile even in traces. Only non-deuterated acetonitrile was detected. On the other hand partially deuterated acetonitrile (but no perdeuterated acetonitrile) could be unequivocally resolved for samples P10 and P15 (which will be discussed in detail in a separate paper).

In the case of methyl amines the situation is complicated by the fact, that not only perdeuterated isotopomers are found but a mixture of amines containing CH_3 and CD_3 groups, which in case of P16 and P17 additionally contain both ^{14}N and ^{15}N (Table 7).

In our recent paper about ^{15}N-labeled PAN homo-polymer[21] we have demonstrated that dimethyl amine is detectable as a volatile stemming from the solvent DMF during the polymer synthesis via chain transfer reaction (exclusively unlabeled $^{14}N(CH_3)_2$-dimethylamino end groups). Thus, dimethyl amine is formed from the end groups (completely unlabeled) or via reaction of ammonia with MA units (containing the $CD_3/^{15}N$-labeling implemented in the material through the monomer choice), while trimethyl amine can be formed from ammonia (which in sample P16 and P17 is ^{15}N-ammonia) and from dimethyl amine formed from the end groups (which always is exclusively $H^{14}N(CH_3)_2$) by reaction with the methyl group of the MA moiety (which in P9 and P16 contains exclusively CD_3 groups). This explains the main tendencies illustrated in Table 7 correctly, in particular those found for mono-methyl amine and dimethyl amine. For trimethyl amine this simple description is not entirely satisfying, since under these assumptions only $^{14}N(CH_3)_2CD_3$ and $^{15}N(CD_3)_3$ should be found in sample P16, and only $^{14}N(CH_3)_2CD_3$ and $^{14}N(CD_3)_3$ should be found in sample P9. However, it is not possible to satisfactorily fit the MS spectra for trimethyl amine of these samples just based on these expected isotopomers (see Figure SI17). Thus, from our results we must propose that additionally a methyl scrambling takes place at least between the mixture of trimethyl amine isotopomers.

However, unequivocally and without any doubt methyl groups of the MA unit are used to form methyl amines in a reaction with ammonia formed during the thermal transformation of the copolymer, while a similar reaction between the MA methyl group and HCN (formed also unequivocally and well-accepted during the thermal transformation of the copolymer) to generate acetontrile can be ruled out on the other hand.

Detailed chemical formation mechanisms will be proposed in the conclusion below.

The amount of formed trimethyl amine using our deconvolution method was between 1–2 mol% relative to the MA content in the starting material. The trimethyl amine is detected simultaneously to ammonia (see Figure SI17).

TABLE 7 Relative amounts of methyl amine isotopomers that best fit the MS spectra (heating rate: 5 K/min)

Sample	$^{14}N(CH_3)_3$ (%)	$^{14}N(CH_3)_2CD_3$ (%)	$^{14}NCH_3(CD_3)_2$ (%)	$^{14}N(CD_3)_3$ (%)	$^{15}N(CH_3)_3$ (%)	$^{15}N(CH_3)_2CD_3$ (%)	$^{15}NCH_3(CD_3)_2$ (%)	$^{15}N(CD_3)_3$ (%)
P9	2	32	27	39	–	–	–	–
P16	1	29	21	10	0	2	12	25
P17	73	–	–	–	27	–	–	–
P5	100	–	–	–	–	–	–	–

	$^{14}N(CH_3)_2H$ (%)	$^{14}NCH_3CD_3H$ (%)	$^{14}N(CD_3)_2H$ (%)	$^{15}N(CH_3)_2H$ (%)	$^{15}NCH_3CD_3H$ (%)	$^{15}N(CD_3)_2H$ (%)
P9	62	0	38	–	–	–
P16	73	0	0	0	0	27
P5	100	–	–	–	–	–

	$^{14}N(CH_3)H_2$ (%)	$^{14}NCD_3H_2$ (%)	$^{15}N(CH_3)H_2$ (%)	$^{15}NCD_3H_2$ (%)
P9	0	100	–	–
P16	0	0	0	100
P5	100	–	–	–

3.3 | Evaluation of the non-volatile polymeric material during the thermal treatment by means of in-situ Fourier transform infrared and solid-state-NMR spectroscopy

3.3.1 | Fourier transform infrared results

Complementary to the analysis of the volatile compounds we also examined the non-volatile main polymeric material during the thermal transformation by means of in-situ-FTIR and solid-state NMR spectroscopy.

In Figure 13 the results of samples P6 (non-labeled), P15 (d^1-AN, d^1-MA) and P11 (d^2-AN) of the in-situ-FTIR measurements are exemplarily shown in comparison extracting four temperatures for each sample (at the beginning of the measurement at 35°C, shortly before the thermal main peak, at top of it, and after the thermal main peak). For the starting AN ν(C≡N) nitrile band at about 2240 cm^{-1} all samples show the behavior that we already have described before in detail for homopolymer PAN.[21] The starting peak at 2240 cm^{-1} disappears with increasing temperature in favor of a new nitrile peak at 2190 cm^{-1} (we did not go to temperatures above 350°C where a third nitrile peak at about 2221 cm^{-1} is expected).

The intensity of the starting MA ν(C═O) carbonyl band at 1732 cm^{-1} decreases more and more with increasing temperature and is completely vanished after the main thermal peak has ceased in all samples.

Concerning the ν(N—H) (and ν[O—H]) bands above 3000 cm^{-1} it is found that for sample P15 before the top of the main thermal peak is reached almost no intensity is detected for them (in comparison to samples P6 and P11). Only at higher temperatures intensity develops in this range, although still decisively lower as compared to P6 and P11. It can be concluded from this finding that the origin of the N—H bonds in the polymeric material is mainly the methine position of the AN-co-MA-polymer, which is in line with the well-accepted tautomerization mechanism for their formation. Taking our proposed formation mechanism for ammonia via regio-specific Hantzsch-type reduction,[21] this also predicts correctly the main tendencies of the found deuteration in ammonia described above, and accepting that the water is formed by reaction of ammonia (or the formed N—H/D moieties within the material) with carbonyl functionalities of the polymeric material, it also predicts correctly the main tendencies for the deuteration in water (however not the minor but substantial contributions from the methylene moieties). Still as mentioned before the parallelism in the deuterium degree might also just be a result of H/D scrambling effects. Thus, the formulated mechanistic conclusions must be taken with due caution, although we think that they are very plausible.

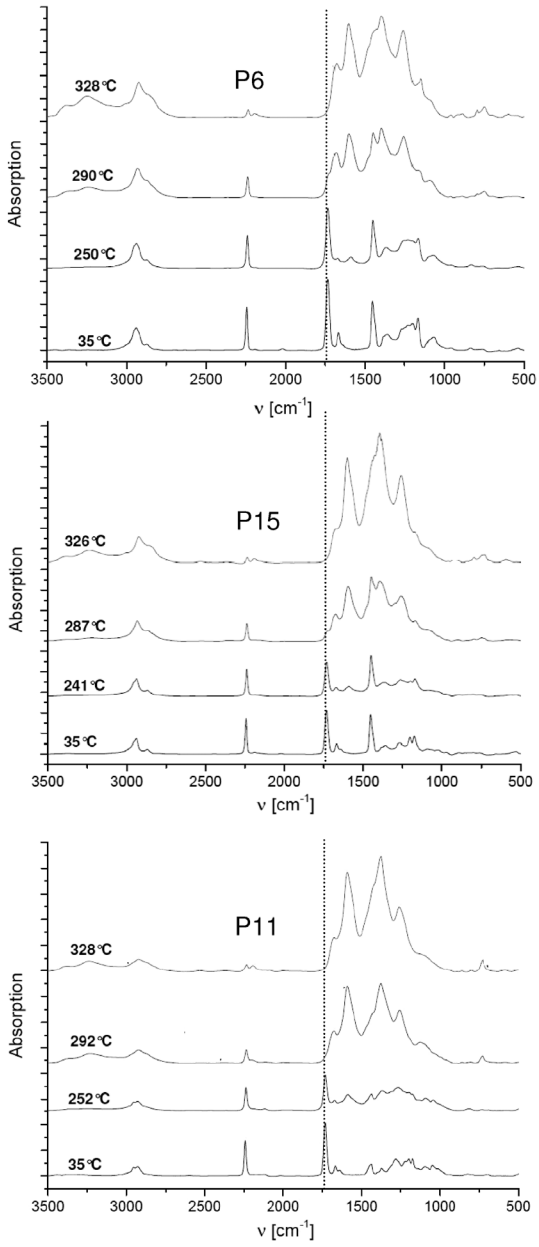

FIGURE 13 Fourier transform infrared spectra of the non-volatile main polymeric materials at four different temperatures for three differently deuterated samples (heating rate: 5 K/min)

We note at this position that the main tendencies in the deuteration degree of the volatile nitriles in the materials of this study are predicted correctly by our proposed mechanism of consecutive Thorpe/Ziegler reaction, retro-hetero-en reaction and regio-specific Hantzsch-type reduction, too, but also in this case a minor but substantial contribution of the methylene moieties is found (and for these volatile nitrile compounds a distorting H/D scrambling is not possible). We will present this in detail in a separate paper, since it would overload this publication.

3.3.2 | Solid-state NMR results

Because of the selective labeling of our samples with ^{2}H, ^{13}C and ^{15}N isotopes, NMR spectroscopy represents a particularly powerful characterization tool of the polymeric solid and it has been applied intensively during this study.

Sample P9 was investigated prior to heating and after having stopped the heating program at 295°C (the sample was transferred immediately from the STA device to the NMR machine for measurement being kept under inert atmosphere during the transport and during the preparation for the NMR measurement; the NMR measurements have been performed at room temperature employing nitrogen as driving and bearing gas). In this sample in particular the fate of the CD_3^{MA} group can be monitored by means of deuterium NMR spectroscopy.

Figure 14 illustrates the ^{2}H-{^{1}H} CPMAS spectra of the starting material (left hand side, top) in comparison to the heat-treated sample (left hand side bottom).

Figure 14 (right) shows the contact time dependence (intensity of the ^{2}H-{^{1}H} CPMAS signal as a function of the Hartmann-Hahn contact time) for the heated and unheated sample. The spinning sideband patterns of the signals for both samples are virtually identical. The envelope of the sideband pattern follows the typical Pake pattern of a nuclear spin with $I = 1$; the quadrupolar coupling constant C_Q for ^{2}H in both samples was determined to 52 ± 6 kHz from the distance of the outermost spinning sidebands. This value is typical for CD_3 groups in which the quadrupolar interaction is partially averaged by the fast CD_3 group reorientation (for the methine and methylene ^{2}H in samples P10 and P11 C_Q was determined to 160 ± 6 kHz).

This indicates that these deuterium atoms do not change their chemical environment dramatically and are still present as CD_3 groups. Since the contact time dependence (cf. Figure 14 right) critically depends on the strength of the $^{1}H - {}^{2}H$ dipolar coupling (for details the reader is referred to a previous paper,[21,29]), the virtual identity of the curves for the unheated and heated sample confirms that also the hydrogen environment of the CD_3 group does not change upon the heat treatment. Quantitative single pulse excitation deuterium measurements revealed that about 41% of initial deuterium is still present in the polymeric bulk material after the heat treatment up to 295°C (i.e., after methanol evaporation has ceased; Figure SI18).

The evolution of the AN-co-MA polymer with temperature triggers distinct changes in the.

^{13}C-{^{1}H} CPMAS NMR spectra for sample P9, as shown in Figure 15.

Two small peaks at 56 ppm (O—CD_3) and 173 ppm (C═O) can be assigned to the −COOMe moiety of CD_3-MA (both in the starting material as well as in the heat-treated polymeric bulk material) while the major peaks show a very similar behavior to that reported by us in a previous paper about the heat-treatment of ^{15}N labeled PAN homopolymer.[21] Thus, the thermal chemical transformation leads to very similar structure motifs for both the PAN homopolymer and the AN-co-MA polymer.

Of particular interest for this study are the solid-state NMR results of sample P17. A ^{13}C-{^{1}H} CPMAS measurement was first performed on the starting material to confirm the peak position of the ^{13}C-labeled carbonyl carbon

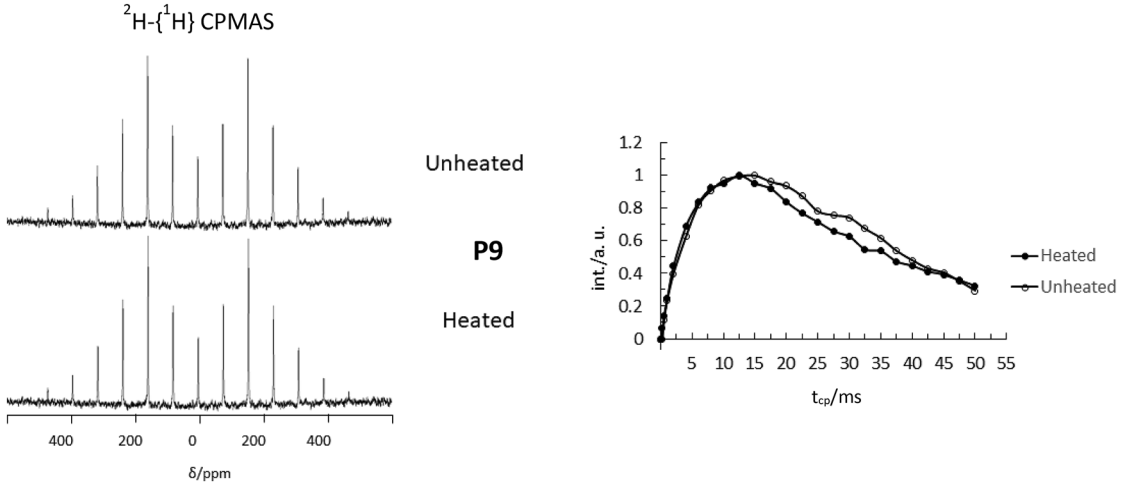

FIGURE 14 Comparison of ^{2}H-{^{1}H} CPMAS (spinning frequency 6 kHz) results of the unheated and heat-treated sample P9 (left hand side) and the dependence of integral signal intensity on the contact time in ^{2}H-{^{1}H} CPMAS experiment (right hand side) measured in a field of 11.7 T. Filled and empty circles represent the integral intensity of the heated probe and the unheated probe, respectively

atom (173 ppm; see FigureSI19) and to estimate the contribution of the non-labeled carbon atoms to the total signal intensity. Then the measurement was performed with the sample heat-treated up to 295°C. The.

^{13}C-{^{1}H} CPMAS spectrum is depicted in Figure 16.

Four main signals can be identified at 149, 152, 163, and 173 ppm with an additional signal of minor intensity at about 137 ppm). The results of the contact time-dependent ^{13}C-{^{1}H} CPMAS study indicate that all major peaks are not directly bound to hydrogen.[21] Quantitative ^{13}C single pulse excitation NMR studies (see Figure SI20) show that the relative ratio of the main peaks at 173, 163 and 152 and 149 ppm (the latter two were treated as one signal in the simulation with DMFIT[30]) are 173:163:(152,149)/70:5:25. An assignment of the main signals to structural motifs will be given at the end of this paragraph after having presented all experimental data.

The results of the ^{15}N-{^{1}H} CPMAS NMR experiments for the heat-treated sample P17 are depicted in Figure 17. The observed spectra are quite similar to those found by us for heat-treated ^{15}N-labeled PAN homopolymer,[21] except for a new pronounced peak at −237 ppm. Two main regions can be distinguished, a region below −200 ppm for nitrogen atoms directly bound to hydrogen atoms (ca. 65%) and a region above −200 ppm for nitrogen atoms with no directly bound hydrogen atom (ca. 35%; relative amounts were determined by a quantitative single pulse excitation; see Figure SI21).

The simultaneous presence of both labels ^{13}C and ^{15}N in sample P17 opens up the possibility to apply dipolar-based NMR experiments to establish proximity or connectivity between the two. One of such experiments is ^{13}C-{^{1}H}-CPMAS-{^{15}N}-REDOR. For details on REDOR the reader is referred to the literature.[31–33] In short, the result from a rotor-synchronized spin-echo experiment

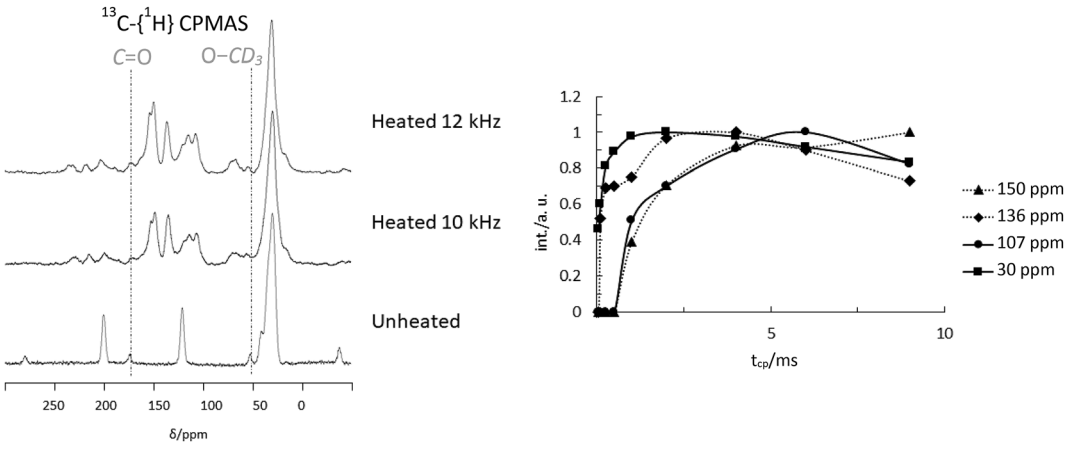

FIGURE 15 Comparison of ^{13}C-{^{1}H} CPMAS results of the unheated and heat-treated sample P9 (left hand side) and the dependence of signal intensity on the contact time in ^{13}C-{^{1}H} CPMAS experiment (right hand side). Triangles with dotted lines, diamonds with dotted lines, circles with solid lines and squares with solid lines represent the peaks located at 150, 136, 107, and 30 ppm, respectively

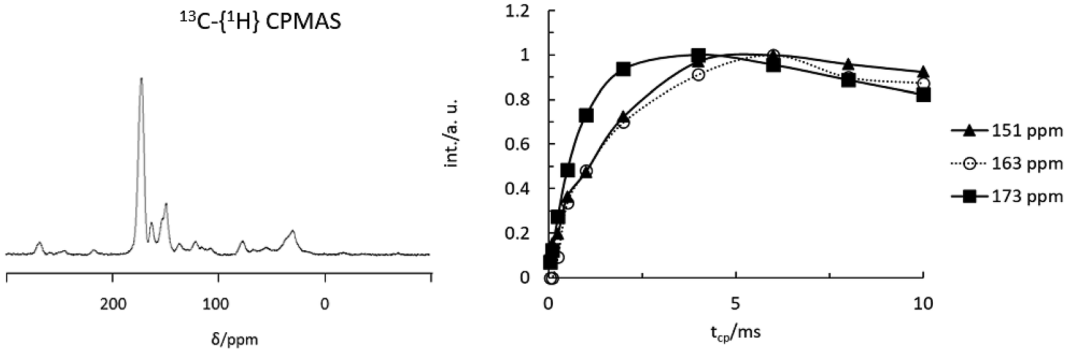

FIGURE 16 ^{13}C-{^{1}H} CPMAS results of the sample P17 heat-treated up to 295°C (left hand side) and the dependence of signal intensity on the contact time in ^{13}C-{^{1}H} CPMAS experiment (right hand side). Triangles with solid lines, empty circles with dotted lines and squares with solid lines represent the signals located at 151 ppm (149 and 152 ppm taken together), 163 and 173 ppm, respectively

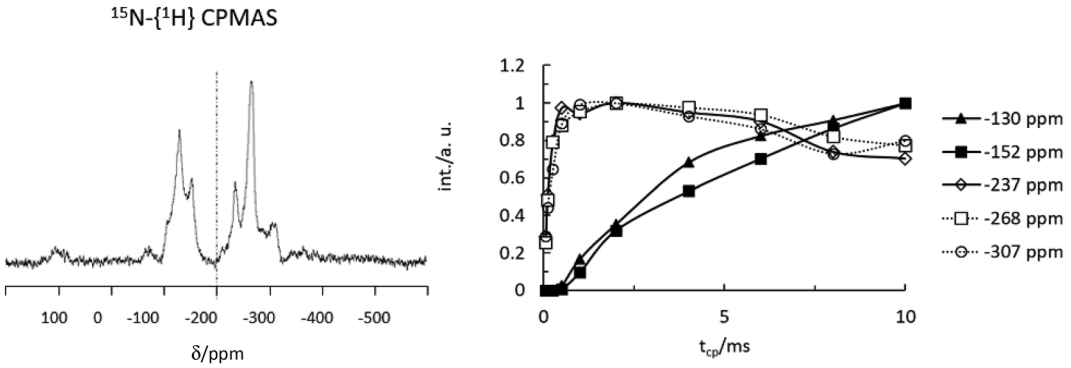

FIGURE 17 ^{15}N-{^{1}H} CPMAS results of the heat-treated sample P17 (left hand side) and the dependence of signal intensity on the contact time in ^{15}N-{^{1}H} CPMAS experiment (right hand side). Triangles with solid lines, squares with solid lines, empty diamonds with solid lines, white squares with dotted lines and empty circles with dotted lines represent the peaks located at −130, −152, −237, −268, and −307 ppm, respectively

for the observed (^{13}C) nuclei, defining the full echo intensity S_0 is compared to a spectrum resulting from an experiment in which the heteronuclear dipolar coupling between ^{13}C and ^{15}N has been re-introduced through rotor-synchronized π pulses on the ^{15}N channel. The difference of the spectra from the two experiments then only contains contributions from ^{13}C nuclei experiencing a dipolar coupling to ^{15}N. The magnitude of the REDOR effect depends on the strength of the dipolar coupling and the dipolar evolution time, the latter of which can be controlled by the number of rotor cycles and the MAS frequency. The resulting REDOR evolution curves can then be analyzed to evaluate ^{13}C-^{15}N internuclear distances. To facilitate the measurements, the ^{13}C-{^{15}N} REDOR is preceded by a ^{1}H → ^{13}C cross polarization step. To the best of our knowledge, this is the first time that this type of experiment has been performed on PAN-based copolymers allowing to estimate the dipolar coupling constants between ^{13}C and ^{15}N nuclei (and thus their distance) within the polymeric bulk material. The low CSA and a good separation of the major signals enabled a quantitative estimation of ^{13}C−^{15}N dipolar coupling constants. Calibration measurements were carried out with ^{13}C/^{15}N double-enriched glycine. The results of the ^{13}C-{^{15}N} REDOR experiment are presented in Figure 18.

All carbon atoms corresponding to the four main ^{13}C peaks (149, 152, 163, and 173 ppm) show a strong dipolar coupling to nitrogen and therefore have nitrogen atoms directly bound to them. Simulation curves were generated employing the SIMPSON software,[28] taking the distance between ^{13}C and ^{15}N atoms to be 1.47 Å (C—N), 1.22 Å (C═N) and 1.11 Å (C≡N) for single, double and triple bonds, respectively, and 1.35 Å (C···N) for single bonds with partial double bond character because of conjugation effects. To simulate the evolution curve for carbon atoms having two nitrogen atoms in the environment, three-spin simulations were performed taking a N—C—N bond angle of 120° into account.

The results of this quantitative simulation propose that the carbonyl carbon atoms corresponding to the peak at 173 ppm are bound to one nitrogen atom through a single bond, possibly with weak partial double bond character. The peak at 163 ppm can be attributed to a carbon atom in a C═C−NH_2 group or to a N—C^{sp2}—N moiety according to the REDOR result. The two peaks at about 151 ppm correspond to C═N and N—C═N structure motifs.

Employing two dimensional heteronuclear correlation experiments it is possible to trace proximity between individual ^{13}C and ^{15}N positions. Spatial proximity between ^{13}C and ^{15}N entails cross peaks in the HETCOR spectrum. Figure 19 shows the result of the ^{13}C-{^{15}N} CPMAS HETCOR experiment.

Six cross peaks show up in the 2D spectrum. From the most dominant cross peak **A** it can be concluded that the carbon atoms being related to the signal at 173 ppm are (at least partly) connected to one nitrogen atom corresponding to the new peak at −237 ppm with directly bound hydrogen atoms. We propose the structure motif **A** in Figure 20 for this constellation or alternatively the tautomeric structure motif **A′**, also depicted in Figure 20, which might even slightly better explain the ^{15}N chemical shift observed. The two cross peaks labeled $\mathbf{S_A}$ were proven to be spinning side bands of **A** and, thus, do not contain additional connectivity information. Cross peak **B** reveals that the carbon atoms giving rise to the signal at 163 ppm are connected to one type of nitrogen atoms (chemical shift: −225 ppm) possessing directly bound hydrogen atoms. We assign this cross peak to structure motif **B** in Figure 20. Alternatively an isolobal structure motif **B′** could be proposed

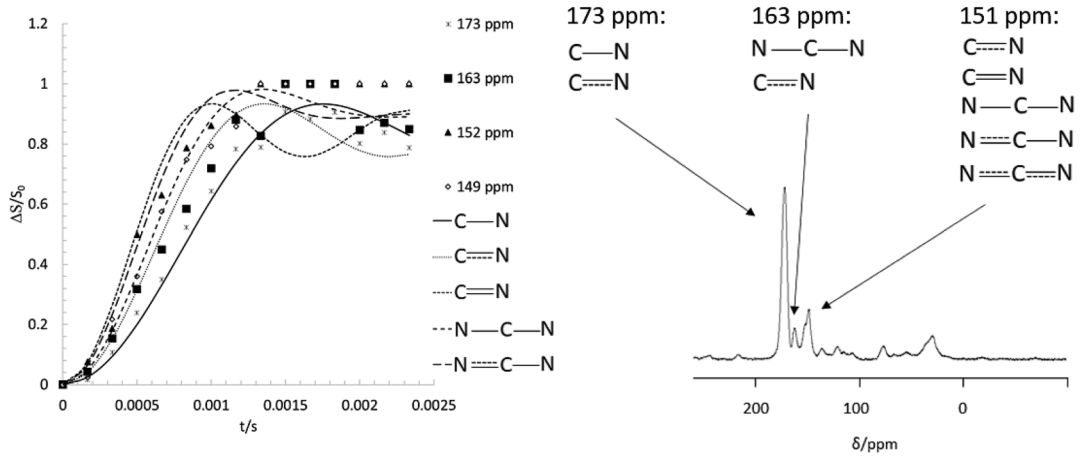

FIGURE 18 Results of ^{13}C-{^{15}N} rotational echo double resonance-evaluation of heated sample P17. Stars, filled squares, filled triangles and empty diamonds represent the experimental results for the peaks at 173, 163, 152, and 149 ppm, respectively. An exemplary spectrum with corresponding peaks marked is represented to the right. Lines represent the results of calibrated SIMPSON simulations[28] with indicated structure motifs

for this constellation. For the carbon atoms related to the signal at 149 ppm (however not to the signal at 152 ppm) support is found for a double-correlation to two different nitrogen atoms with chemical shifts at −152 ppm (no directly hydrogen atoms bound) and at −268 ppm (with directly bound hydrogen atoms). We attribute this constellation to the amidine structure motif $\mathbf{C^{1/2}}$ in Figure 20. Again, an isolobal structure motif such as $\mathbf{C1'}$ in Figure 20 cannot be completely ruled out as reason for the cross peak $\mathbf{C^1}$ in Figure 19. In that case the double-correlation would be partially coincidentally. However, cross peak $\mathbf{C^2}$ cannot be explained by this structure motif.

Structure motifs **B** and **C** in the large box of Figure 20 are remarkable in so far as they do not contain any oxygen bound to the labeled carbon, which will be explained in the conclusion section. We note further that free carboxylic amide structure motifs as shown in gray color in Figure 20 cannot be detected or supported by the HETCOR experiment.

Taking these findings, one main conclusion about the fate of the MA repeat unit on thermal treatment is that (at least partly) the ester is transformed to a carboxylic amide (by reaction with ammonia) which itself is not stable at 295°C, however it starts the well-established cyclization reaction cascade leading to structure motifs **A**, **B**, and **C** in Figure 20.

To further support this conclusion, we performed additional experiments on sample P18, which already contains the carboxylic amide functionality in the first place. We performed ^{15}N-{^1H} CPMAS (Figure 21) and ^{13}C-{^1H} CPMAS (Figure 22) measurements with two heat-treated samples (the thermal treatments were interrupted at two

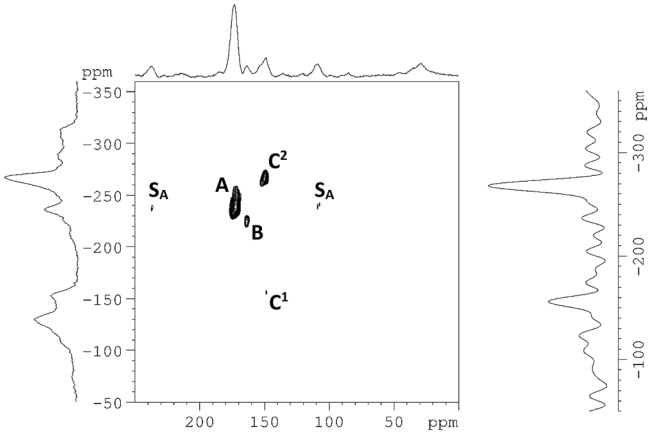

FIGURE 19 ^{13}C-{^{15}N} CPMAS HETCOR NMR 2D spectrum of the heat-treated sample P17. Spectra to the left and at the top represent the ^{15}N-{^1H} (left) and ^{13}C-{^1H} CPMAS NMR spectrum (top). The spectrum at the right represents a slice parallel to the ^{15}N dimension at a ^{13}C chemical shift position of 149 ppm

different temperatures, one directly after the main thermal peak at 230°C, where the main thermal transformation has ceased in sample P18, and one at 320°C which represents a temperature where the main thermal transformation has ceased in the AN-co-MA polymer).

Figure 21 shows that the same new pronounced signals at −224 and −235 ppm are observed as with the AN-co-MA-polymers even when the heating is stopped at 230°C. The contact time behavior of those two signals is identical. The highest intensity of the peak at −235 ppm in sample P18 supports the proposal of structure motif **A** in Figure 20. At 320°C the same main peaks are found in the spectrum below −200 ppm as for sample P17. Almost no

intensity is found above −200 ppm. From this fact it can be concluded that no pronounced scrambling of the carboxylic amide nitrogen atoms along the chain takes place (but a little bit it does, which will be explained below), and almost all pyridyl/amidinyl-type nitrogen atoms without bound protons stem from the nitrile groups which are unlabeled and, thus, not visible in the spectrum. These aspects give strong evidence for our proposal that the carboxylic amide, formed from the MA moiety by reaction with ammonia, is an intermediate in the thermal transformation of AN-co-MA polymers. The ^{13}C-{^{1}H} CPMAS spectrum in Figure 22 additionally confirms this conclusion, being very similar to the spectrum depicted in Figure 15.

We note that sample P16 was also initially planned for dipolar-based NMR experiments. However, at the moment the present NMR hardware does not allow to simultaneously tune to ^{15}N and ^{2}H. We hope to be able to perform these experiments in the future.

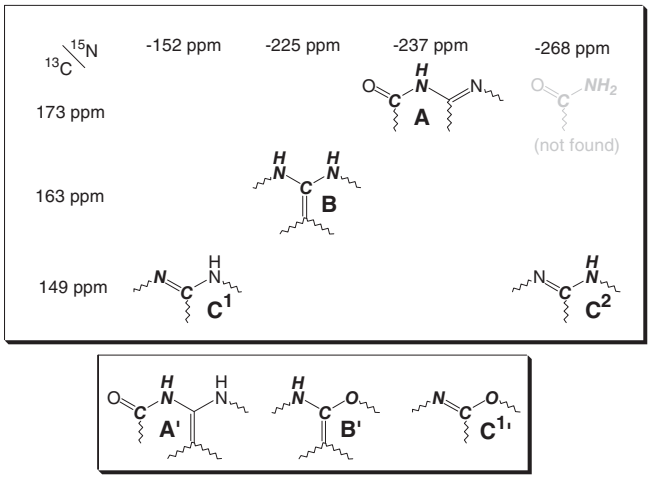

FIGURE 20 Assignments of the ^{13}C and ^{15}N NMR peaks in sample P17 to structure motifs based on results of the HETCOR experiment

3.4 | Model compounds

One important elemental reaction in case of the thermal treatment of PAN homopolymer has been shown by us to be the Ziegler/Thorpe reaction.[21] We synthesized ^{15}N-labeled model compounds to elucidate the spectroscopic behavior, connected with the functionalities formed (Figure 23; **D**). Consequently, in case of the AN-co-MA polymer the analogous Diekmann condensation (Figure 23; **A**) should play a similar role as well as the mixed Diekmann/Thorpe/Ziegler-type reactions between esters and nitriles (Figure 23; **B** and **C**). With the series of model compounds in Figure 23 we are able to challenge all possible constellations and determine the

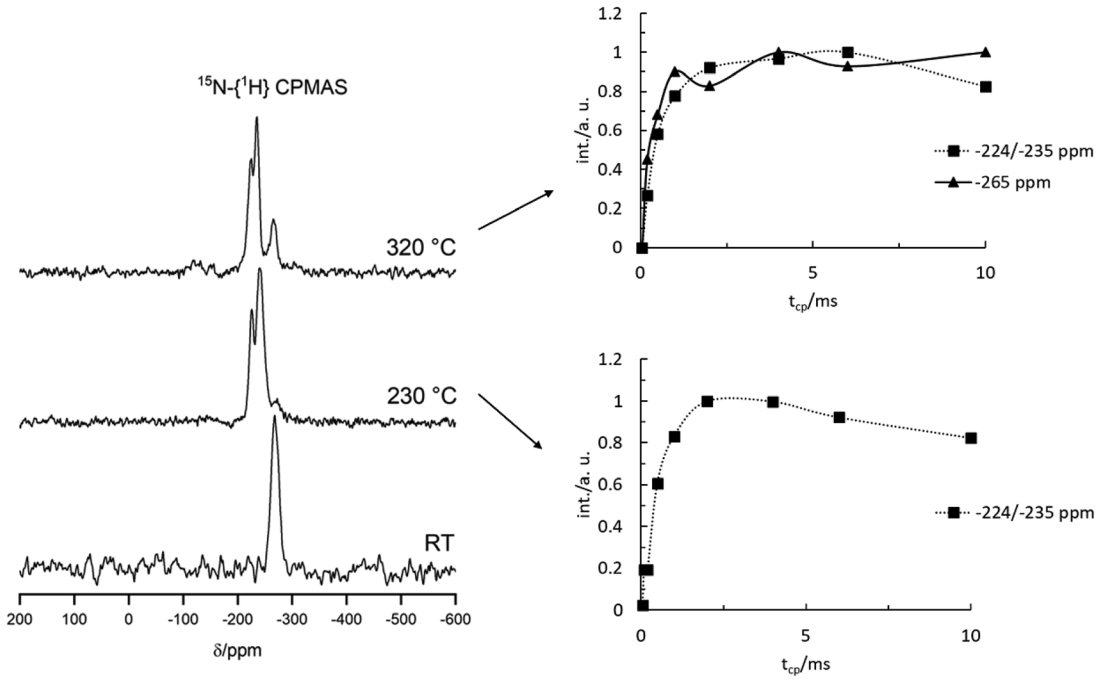

FIGURE 21 ^{15}N-{^{1}H} CPMAS results of sample P18, starting material, heat-treated until 230°C and heat-treated until 320°C (left hand side) and the dependence of signal intensity on the contact time in the ^{15}N-{^{1}H} CPMAS experiment (right hand side: Bottom: 230°C; top: 320°C) measured in the field of 7.05 T. filled squares with dotted lines and filled triangles with solid lines represent the peaks located at −224, −235, and −265 ppm, respectively

spectroscopic data to be expected for them in the polymeric material during the thermal treatment.

The synthesis way for the new compounds **A** and **B** is shown in Figure 24. Details about the synthesis and characterization are given in the Figure SI22. An ORTEP plot of a molecule in the solid state resulting from a single crystal X-ray analysis of compounds **A** and **B** is shown in Figure 25. In the crystalline solid both compounds are present exclusively in the enol form (respectively enamine form) with a hydrogen bond between the enol —OH (respectively the enamine —NH_2) and the carbonyl oxygen of the ester moiety. In addition, in solution exclusively the enol/enamine tautomer is observed. The spectroscopic data of the model compounds are listed in Table 8 (for compound $\mathbf{P^{MA}}$ see Figure 26).

An important feature is that while the NMR spectroscopic data for the —COOMe moiety do not change strongly, a pronounced decrease in the wavenumber for the ν(C═O) stretching vibration is found in the FTIR measurement for model compounds **A** and **B** because of the +M-effect of the conjugated enol/enamine functionality. This is in accordance with the finding that in the heat-treated polymer still methyl ester functionalities can be detected via solid- state NMR spectroscopy while at the same time the peak for the ν(C═O) stretching vibration of the starting material at 1732 cm^{-1} vanishes completely on heat treatment.

Since some of our results point to the fact that a N/O-scrambling within the cyclized polymeric material takes place, we wanted to challenge this question with a model compound. We therefore synthesized model compound $\mathbf{P^{AA}}$ according to the reaction pathway depicted in Figure 26 (for detailed synthesis information see Figure SI23).

This model compound corresponds to AA (acrylic acid) as comonomer rather than MA. If this compound is heat-treated at 200°C for 1 h a rearrangement including N/O-scrambling takes place in a clean reaction (Figure 27). Single crystals of the reaction product suitable for X-ray analysis could be grown from diethyl ether

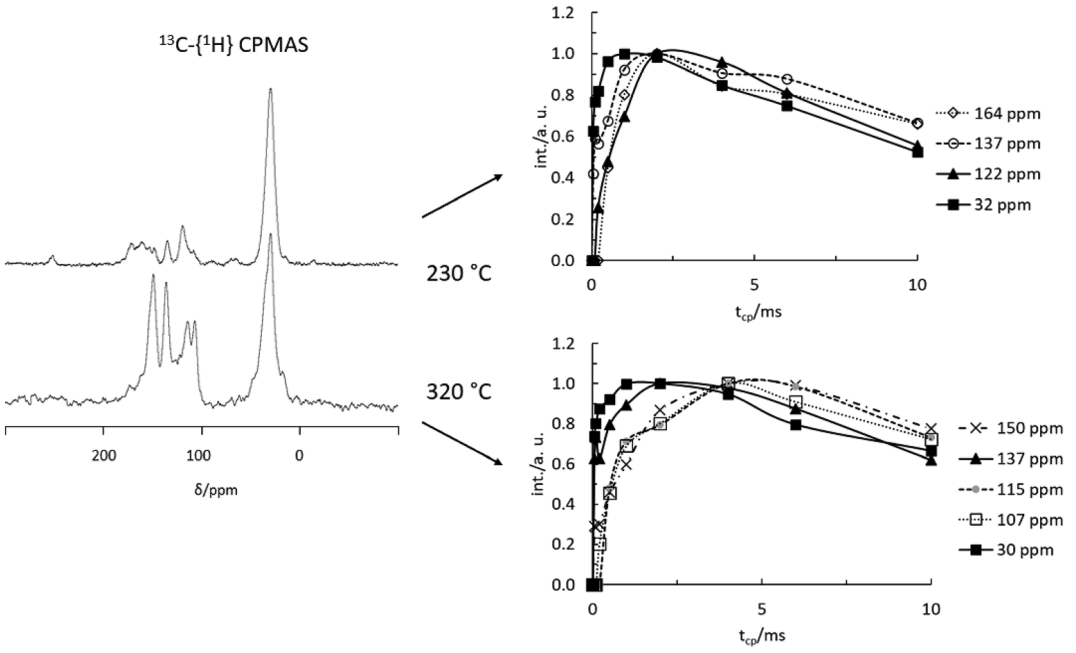

FIGURE 22 ^{13}C-{^{1}H} CPMAS results of sample P18 heat-treated up to 230°C and 320°C (left hand side) and the dependence of the signal intensity on the contact time in the ^{13}C-{^{1}H} CPMAS experiment (right hand side: Bottom: 320°C; top: 230°C)

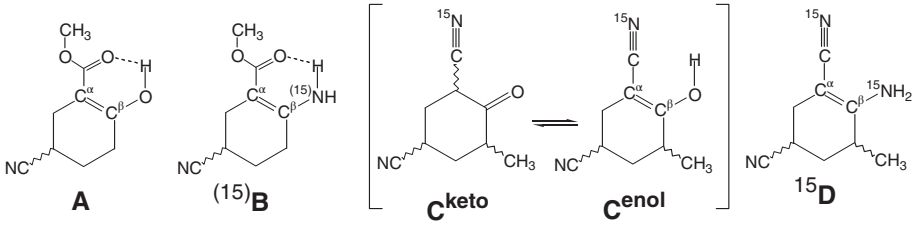

FIGURE 23 Model compounds synthesized in the course of this and a previous study by us

and an ORTEP representation of a molecule in the solid state is shown in Figure 28. We note that model compound $\mathbf{P^{MA}}$ is stable under the same conditions (200°C, 1 h).

Some interesting aspects can be concluded from this reaction behavior:

1. The formation of $\mathbf{P^{200}}$ serves as a proof of principle for the existence of N/O-scrambling, and this scrambling is fast in comparison to a further cyclization reaction.
2. Mobile acidic protons are required for the initiation of the cyclization reaction. The ester moiety itself cannot initiate the cyclization reaction.
3. The oxo group of the imido carbonyl function does not easily continue the cyclization (we propose that in the polymeric material an aminate is formed prior to a cyclization via reaction of ammonia with the carbonyl oxo and that in any way ammonia serves as a catalyst for the cyclization and its initiation (see Figures 30 and 31).
4. Because of the preceding conclusion structure motifs $\mathbf{B'}$ and $\mathbf{C^{1'}}$ in Figure 20 are less likely, although we cannot exclude them completely.

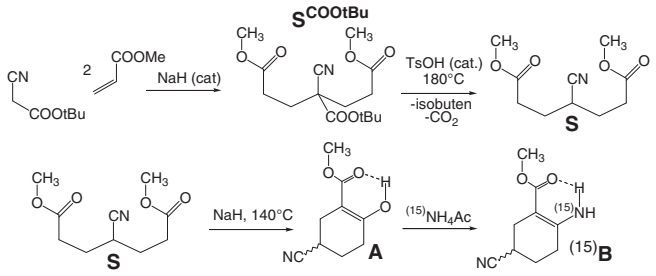

FIGURE 24 Synthesis pathway for the new model compounds of this study

4 | MECHANISTIC CONCLUSIONS DRAWN FROM THE RESULTS

Taking all the results of this study we are now in the position to formulate a deeper insight into the chemical transformation mechanisms connected with the MA unit of the AN-co-MA-polymers during their thermal treatment.

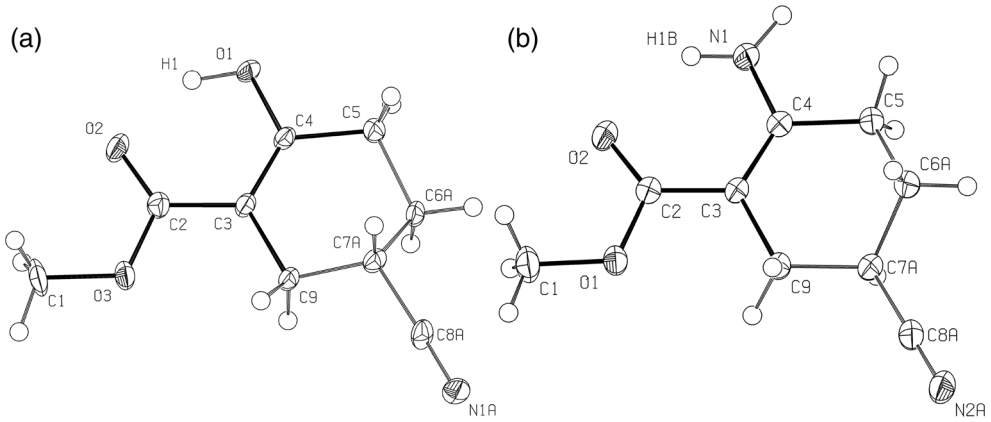

FIGURE 25 ORTEP representation of (a) compound **A** and (b) compound **B**, collected at $T = 100(2)$ K. Thermal ellipsoids are drawn at the 50% probability level

TABLE 8 Spectroscopic results for the model compounds in comparison (copolymer NMR data in dmso-d^6; ^{15}**B** NMR data in toluene-d^8; all others in $CDCl_3$)

Compound	CH_3^{MA} (ppm)	$C{=}O^{MA}$ (ppm)	$C{\equiv}N^{AN}$ (ppm)	C^{α} (ppm)	C^{β} (ppm)	NH_2 (ppm)	ν(C=O) (cm^{-1})	ν(C≡N) (cm^{-1})
Copolymer[a]	52.4	174	120.5	–	–	–	1732	2242
S	51.9	172.5	120.7	–	–	–	1731	2241
P^{MAa}	52	175	120	–	–	–	1730	2242
A	51.7	171.9	121.3	94.8	170.5	-	1656	2241
^{15}B	50.2	169.4	121.5	88.5	154.7	−301	1666	2237
$^{a}C^{keto}$	–	–	119	–	–	–	1728	2244
D[a]	–	–	120	71	158.5	−311	–	2245/2179

[a]Several stereo-isomers present with slightly different chemical shift.

To start with we notice that all main assumptions about the elemental reactions involved in the thermal transformation mentioned in our previous paper about ^{15}N-labeled PAN homopolymer were confirmed during this extended study (several aspects about the volatiles stemming from the AN unit will be presented in a following separate paper). We now will present detailed chemical mechanisms to explain the findings of this paper and will sum up with a semi-quantitative master map (Scheme 1) for all main processes involved.

4.1 | Formation of methanol

We propose that the formation of methanol runs via two pathways, both of them strongly connected with ammonia acting as stoichiometric reagent in one case and as catalyst in both cases. The first pathway is an amidation (Figure 29) or amidination (Figure 30) of the MA ester functionality by ammonia (acting as both a stoichiometric reagent and as catalyst). Supported by our results, we propose that these reactions run via ammonia that is bound to the polymeric chain by means of hydrogen bonding. Four elemental processes are possible for this ammonia. The hydrogen bond can be cleaved leading to the evaporation and, thus, loss of ammonia (α in Figure 29). The ammonia can migrate along the polymeric chain without complete cleavage of the hydrogen bond (β in Figure 29). The ammonia can react with the nitrile or ester functionality as a Lewis base (γ in Figure 29). Alternatively, the ammonia can react with the most acidic protons at the methine positions as a Brönsted base (δ in Figure 29).

The key elemental reaction for the amidation and amidination is pathway γ in Figure 29, which according to the proposed mechanism requires at least two ammonia molecules (one as reagent and one as catalyst) per methanol formation step.

Alternatively, methanol can be formed in the course of a classical Diekmann-analogous condensation reaction (Figure 31) with ammonia as Brönsted-basic catalyst (pathway δ in Figure 29). We propose that the thermodynamic driving force for this reaction cascade is the consecutive hetero-en-reaction, leading to a structure motif similar to model compound **C** in Figure 23. Since no keto function could be detected by IR spectroscopy it is proposed that a fast reaction of ammonia with the keto function leads to the final enamine moiety similar to model compound **B** (Z = —COOMe in Figure 31) or **D** (Z = —CN in Figure 31) from Figure 23 along with water release.

The mechanism shown in Figure 31 would also explain the preference of the MA methine position (Z = —COOMe in Figure 31; $pK_a \approx 25$) over the AN methine position (Z = —CN in Figure 31; $pK_a \approx 30$).

The reaction cascade in Figure 31 also explains correctly the consecutive deuterium transfer mainly from the methine position (preferably from the MA unit) from the

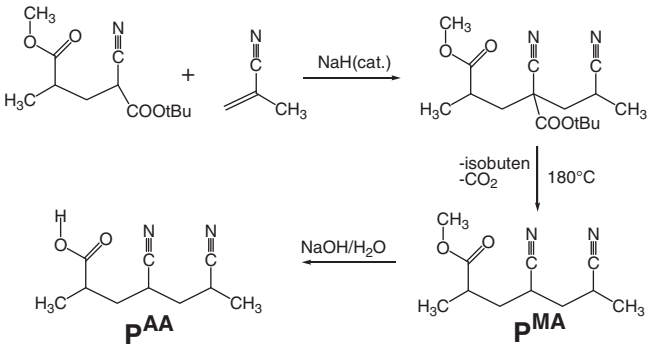

FIGURE 26 Synthesis pathway for the new model compound $\mathbf{P^{AA}}$

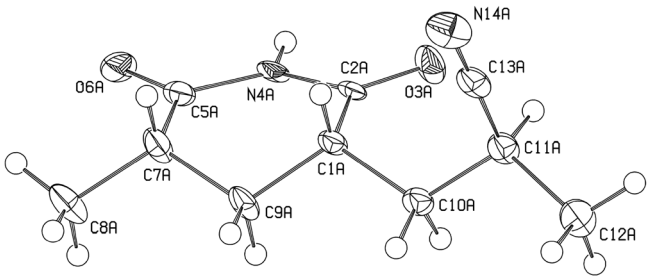

FIGURE 28 ORTEP representation of compound $\mathbf{P^{200}}$ $C_{10}H_{14}N_2O_2$ (major diastereomer), collected at $T = 100(2)$ K. Thermal ellipsoids are drawn at the 50% probability level

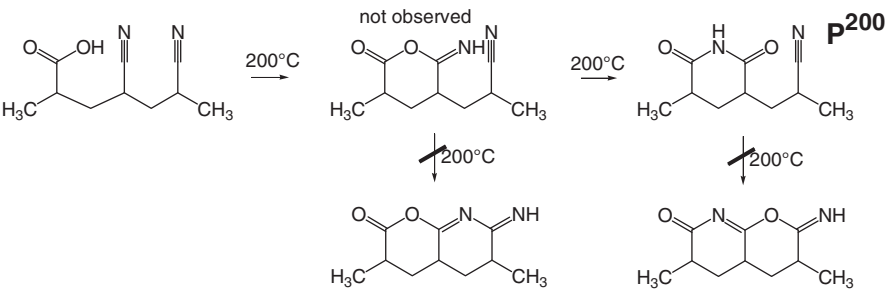

FIGURE 27 Thermal transformation including N/O-scrambling on heating $\mathbf{P^{AA}}$ to 200°C for 1 h

bulk starting material to ammonia and from ammonia to methanol respectively water. It fails though to explain the contribution of the methylene moiety as deuterium source.

The best mechanistic explanation for this experimental finding that we can provide, is a chemical H/D scrambling between layers of tautomerized bulk solid materials as depicted in Figure 32, which then translates further into the other compounds via the already formulated and published consecutive reaction pathways.

This explanation would be in accordance with the found preference towards an AN methylene group concerning this effect.

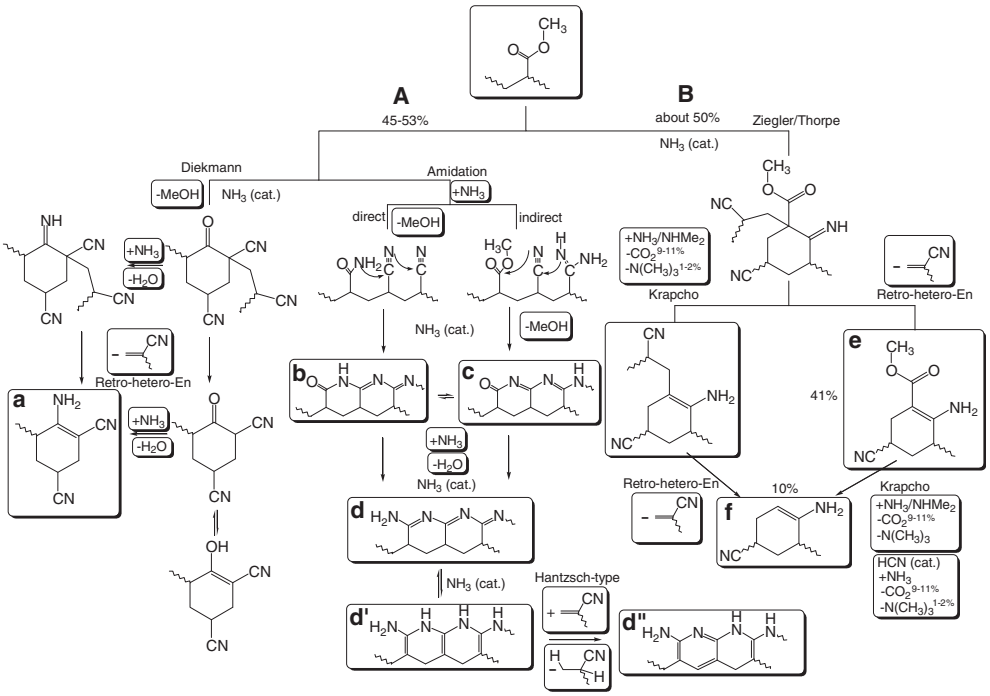

SCHEME 1 Master scheme containing all main reaction pathways

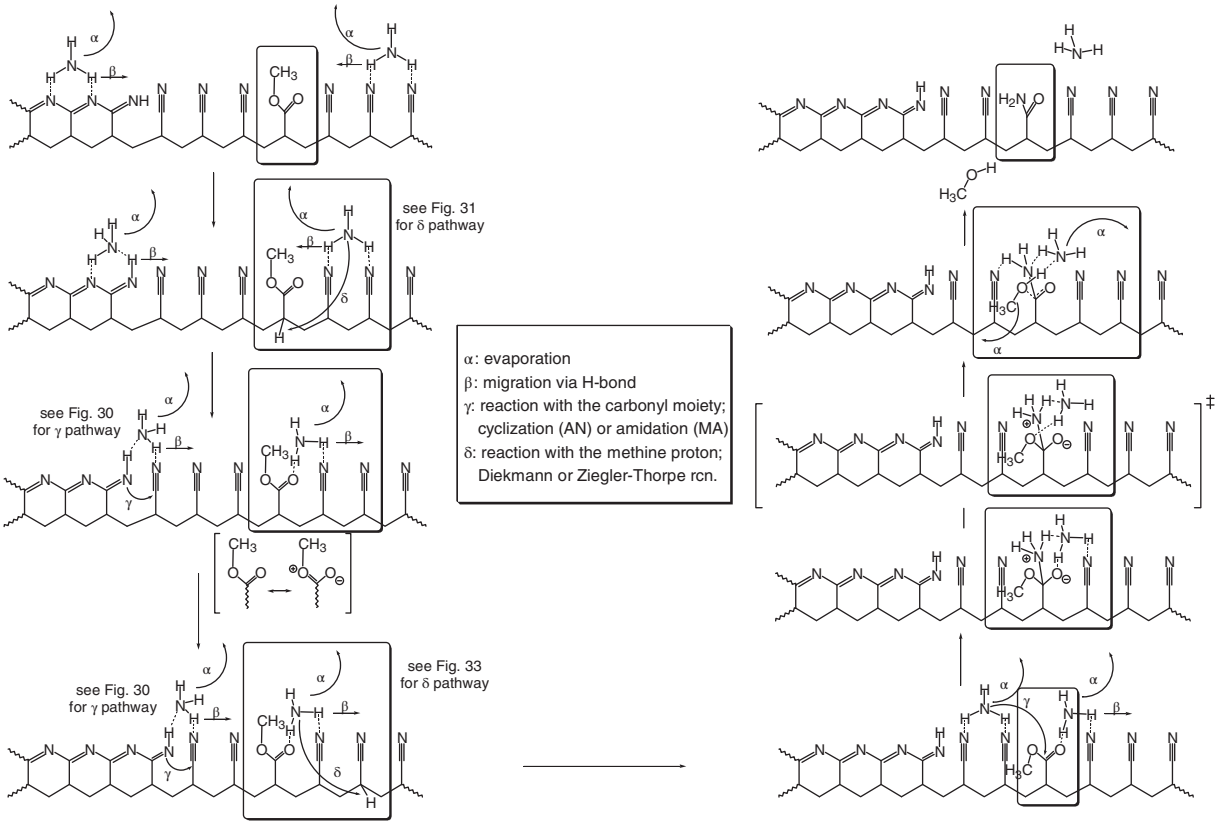

FIGURE 29 Direct amidation mechanism leading to methanol

4.2 | Formed functional groups in the polymeric material

For the heat-treated polymeric material we found that still methyl ester functionalities are present (NMR spectroscopy), however in a different electronic environment as compared to the starting material (IR spectroscopy). We propose that this is because of a Diekmann reaction as shown in Figure 31 with Z = —COOMe or a Ziegler/Thorpe-analogous reaction pathway, again followed by a hetero-en-reaction as thermodynamic driving force (Figure 33).

Both reaction pathways lead to structure motifs similar to model compound **B** from Figure 23. The determined spectroscopic data for this model compound are in accordance with the spectroscopic data found for the heat-treated copolymer.

4.3 | Formation of CO_2 and methyl amines

We propose that carbon dioxide is formed via a Krapcho or Krapcho-analogous reaction from structure motifs similar

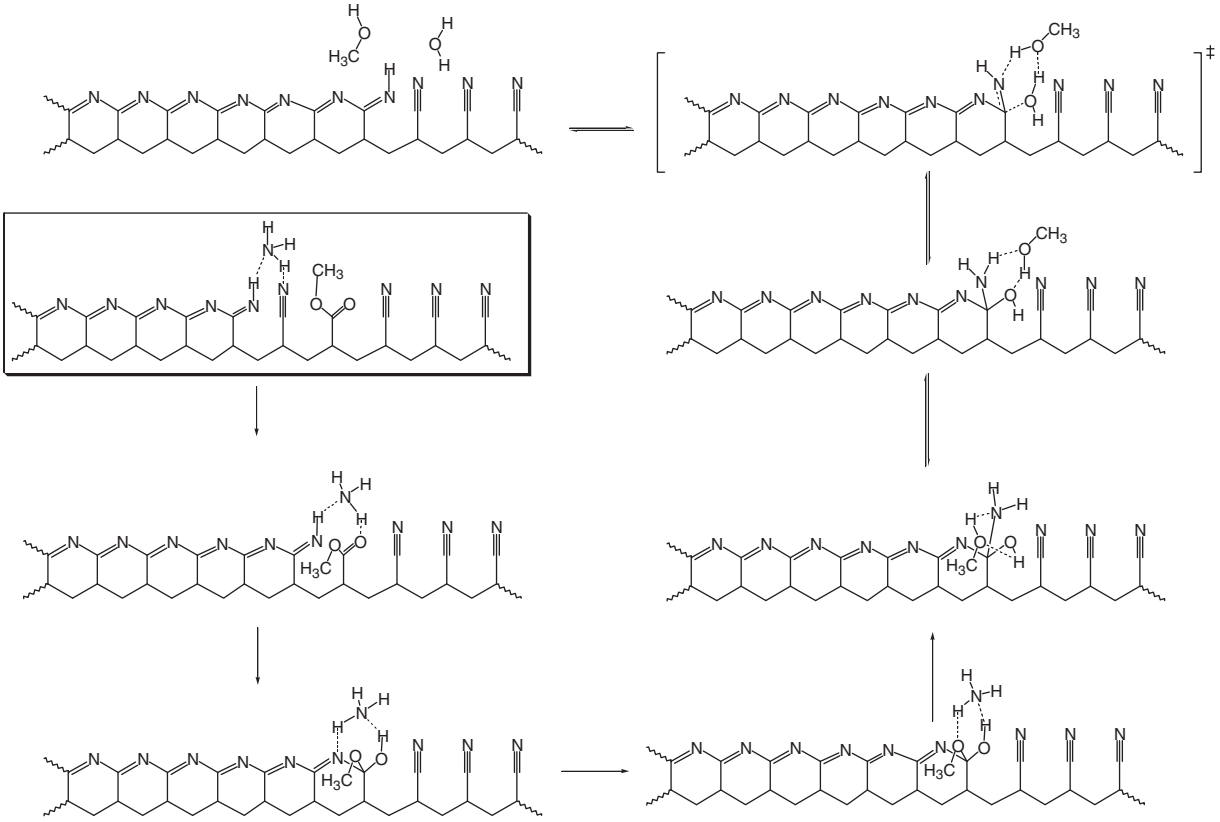

FIGURE 30 Indirect amidination mechanism leading to methanol and water

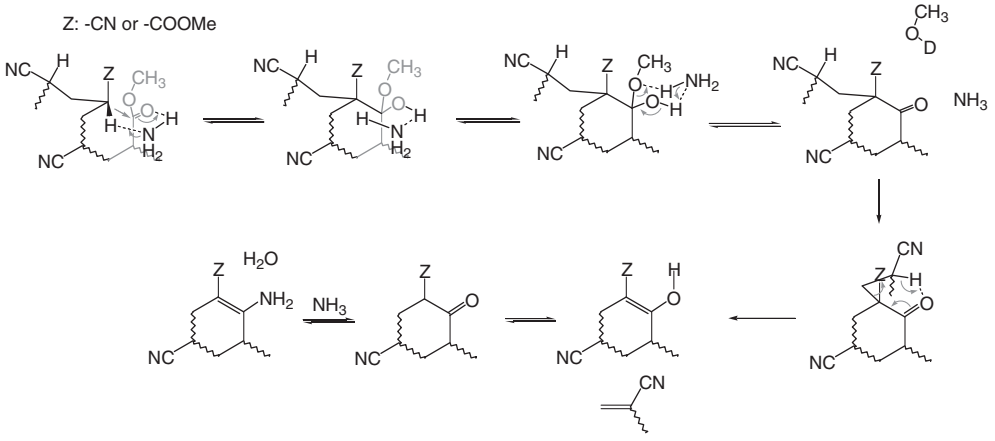

FIGURE 31 Diekmann-analogous reaction pathway leading to the formation of methanol and water (of course, the reaction does not necessarily need to run via a six-membered ring)

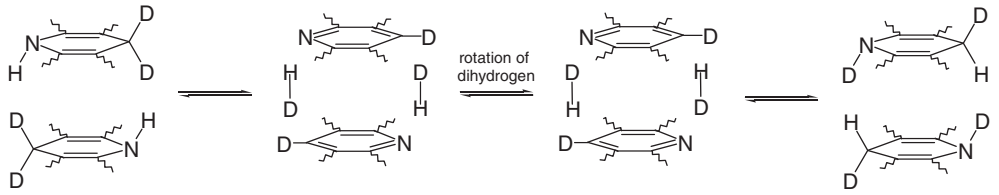

FIGURE 32 Possible explanation for the contribution of deuterium stemming from the methylene positions of the bulk starting material via chemical H/D scrambling between tautomerized layers of the solid

FIGURE 33 Ziegler/Thorpe-analogous reaction pathway leading to the formation of methyl esters conjugated to a NH_2-group

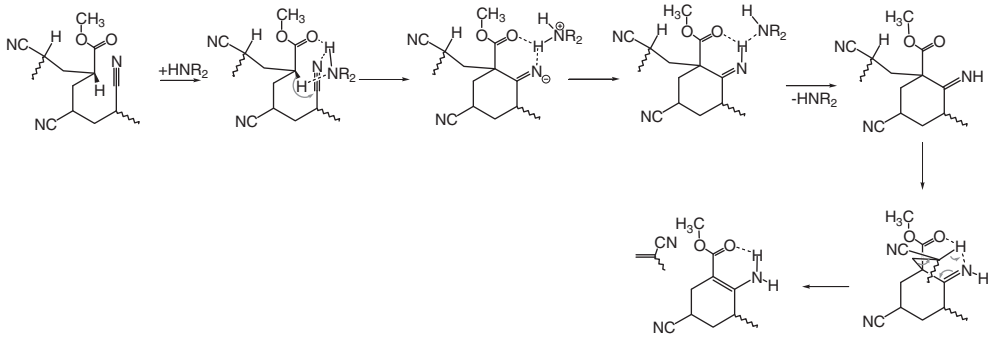

FIGURE 34 Krapcho reaction pathway leading to the formation of carbon dioxide (without the formation of acetonitrile)

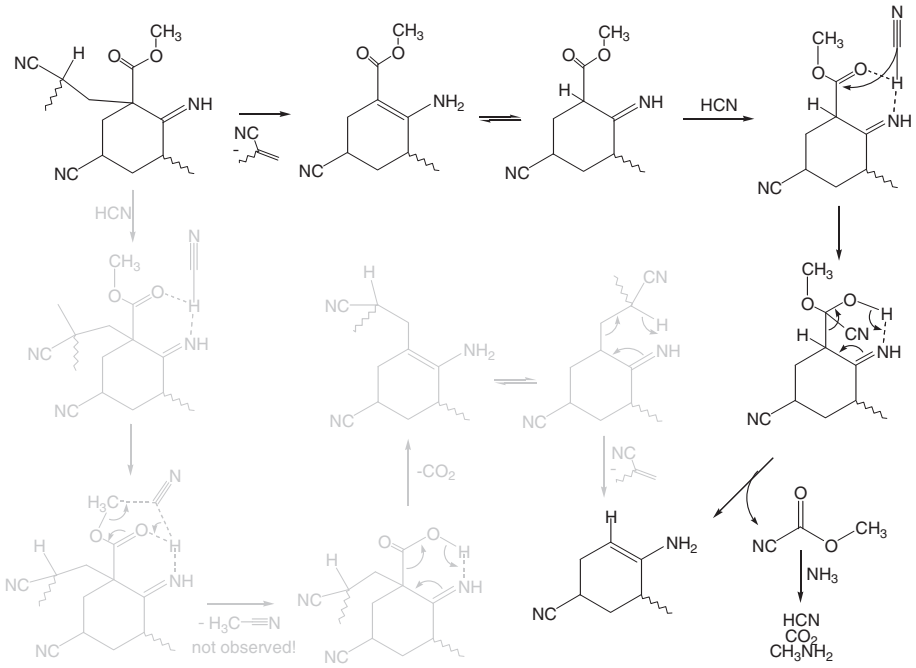

to model compounds **A** and **B** in Figure 23 (Figures 34 and 35). For the classical Krapcho reaction[34–36] with cyanide anions two mechanisms have been reported. Since no per-deuterated acetonitrile was detected, one of them can be excluded which concerning the sterics in the structure motif is in accordance with the original paper of Krapcho (Figure 34).

We propose that a Krapcho-analogous reaction with amines containing at least one N—H bond instead of HCN acting as reagent will also (maybe even favored over the reaction pathway in Figure 34 with HCN) lead to the formation of carbon dioxide and the different detected methyl amines (Figure 35). This type of reaction is literature-known..[37–39]

The amount of about 10 mol% CO_2 relative to the MA content in combination with the found 1–2 mol% of trimethyl amine (not to count the also detected mon- and dimethyl amine) are in accordance with this mechanism and support that the main contribution is from the Krapcho-analogous reaction in Figure 35.

Since the amount of formed carbon dioxide is smaller than the amount of still present methyl ester, the decarboxylation of structure motifs **A** and **B** from Figure 23 is a minor reaction under the applied conditions of thermal treatment.

4.4 | Nitrogen/nitrogen and nitrogen/oxygen scrambling

From Figure 21 evidence was found that to a minor degree N/N scrambling occurs along the polymer chain backbone. One possible mechanism for this scrambling is depicted in Figure 36. We note that an alternative explanation for the NMR results can be given by a tautomerization mechanism also shown in Figure 36 without N/N scrambling, and since more than one peak is found in the range of −150 to −200 ppm in Figure 21 also both pathways might be active (because of the several peaks it is unlikely that only the tautomerization takes place).

Similarly, the NMR results shown in Figures 19 and 20 suggest that a nitrogen/oxygen scrambling along the polymeric chain possibly takes place. We propose a similar mechanism for this scrambling to the one mentioned in Figure 36 (Figure 37). The occurrence of the nitrogen/oxygen scrambling is supported by the results found with model compound $\mathbf{P}^{\mathbf{AA}}$ (Figure 37). However, the observation of structure motifs **B** and **C** from the large box in Figure 20 without bound oxygen on the labeled carbonyl carbon can alternatively also be explained by simple amidination reaction of ammonia with the firstly formed amide.

Still unanswered is the question how the high amount of unlabeled carbon dioxide can be explained in the thermal treatment of sample P17.

The O/N scrambling followed by re-addition of formed methanol might be involved in this process (Figure 38 top).

In addition, a re-addition of formed methanol and water to a nitrile moiety is a possible pathway for the formation of unlabeled CO_2 in sample P17 (Figure 38 bottom).

A possibility to prove this mechanism is by examining a sample being ^{13}C labeled at the nitrile carbon rather than the ester carbonyl carbon. However, this experiment will remain for the future.

5 | FINAL CONCLUDING REACTION SCHEME AS QUINTESSENCE OF THIS STUDY

We reach now to a point where we want to summarize the main conclusions of this study in one single reaction scheme (Scheme 1).

The motor for several reaction pathways, including in particular the cyclization reaction, according to our proposal, is ammonia, which acts as both initiator and catalyst. According to this study the formation of the ammonia is in agreement with our proposed Hantzsch-type reduction[21] and thus independent of the MA

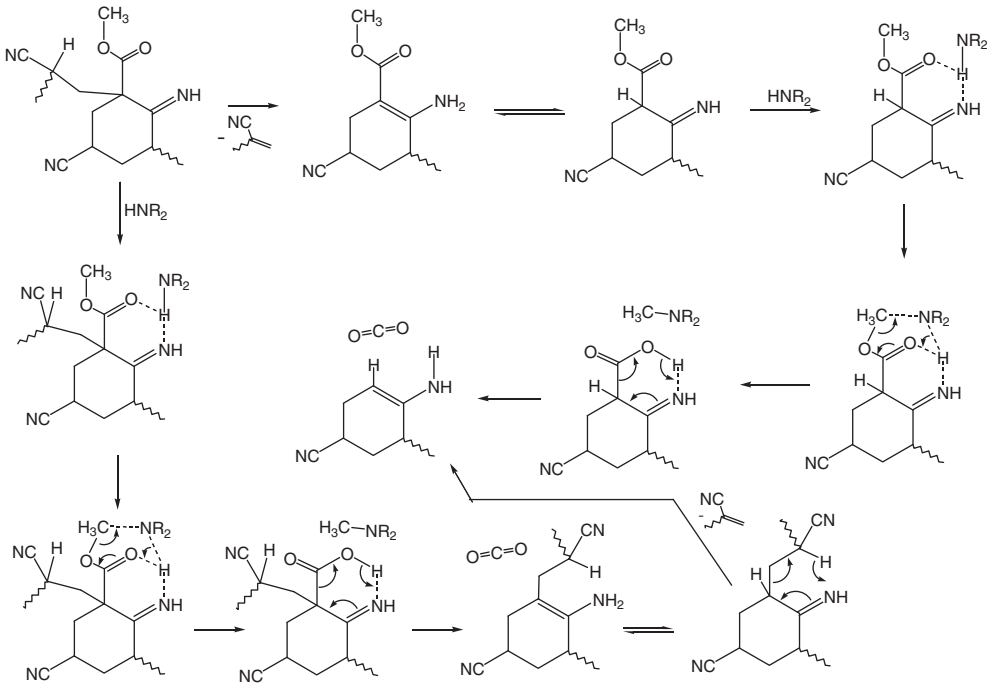

FIGURE 35 Krapcho-analogous reaction pathway with amine instead of HCN attacking reagent

moieties. However, parts of the ammonia molecules are consumed in the reaction with the MA unit either directly or indirectly (reaction pathway **A** in Scheme 1), forming carboxylic amide functionalities and in last instance amidine functionalities or enamine moieties which are indistinguishable from the functionalities formed by PAN homopolymer. This, according to our proposal, is the reason why MA as a comonomer shifts

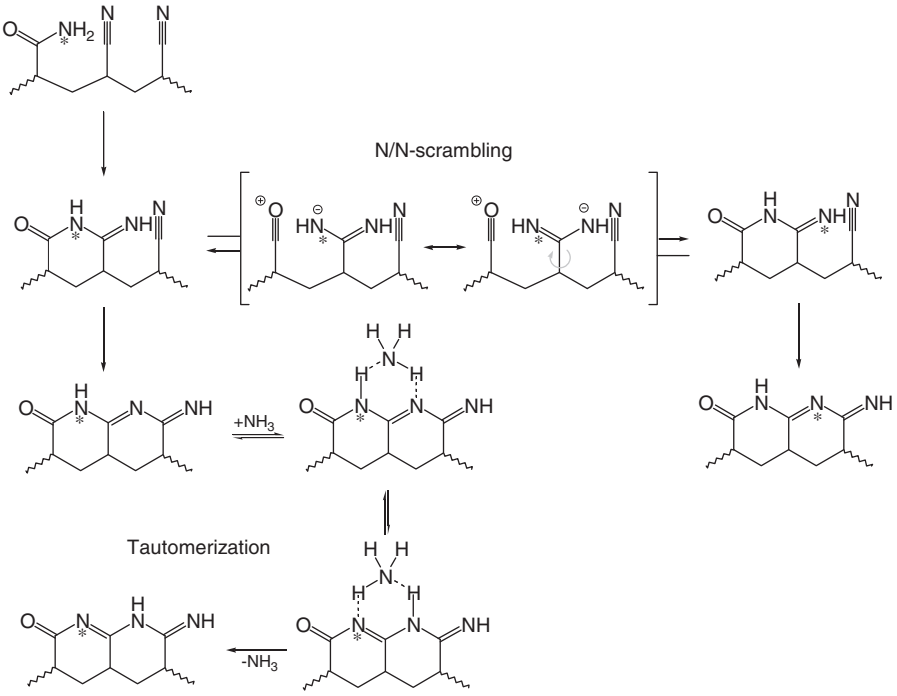

FIGURE 36 Proposed mechanism for the N/N scrambling found in the polymeric material

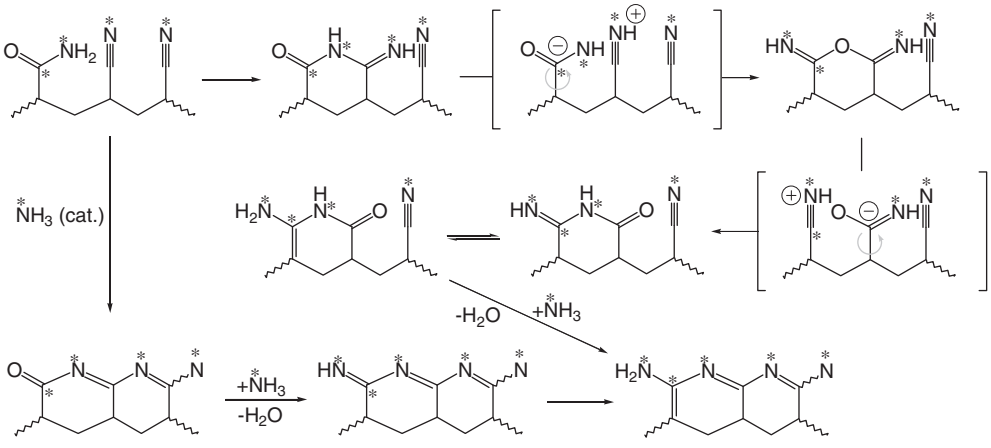

FIGURE 37 Proposed mechanism for the O/N scrambling found in the polymeric material

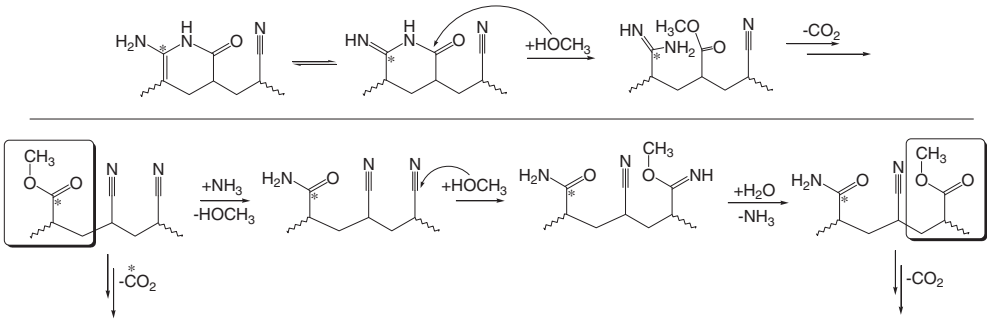

FIGURE 38 Proposed mechanisms for the formation of unlabeled CO_2 from sample P17

the thermal transformation, in particular the highly exothermic cyclization reaction, to higher temperatures as compared to PAN homopolymer (lower concentration of initiator/catalyst ammonia in the AN-co-MA polymer). In spite of this, and actually as a consequence, however, the MA moiety in last instance does not act strongly as a perturbating structure element within the thermally stabilized polymeric material compared to PAN homopolymer.

Thus, the AN-co-MA precursor can in fact be considered a smart material in which the MA moiety supports the drawing process at low temperatures while at higher temperatures it switches self-dependently to an amide or enamine functionality by reaction with self-formed ammonia, which then supports the cyclization reaction, ending up with the same structure motifs as, found for PAN homopolymer.

According to this study two main reaction pathways **A** and **B** in Scheme 1 are active. Along the main reaction pathway **A** methanol and water are released in approximately the same amount. Since the overall yield of methanol approaches a value of 45%–53% at MA contents between 5–10 mol%, we conclude that about 45%–53% of all MA transformations follow this route. Route **A** splits further off into two sub-branches, one connected with the well-established cyclization mechanism (which according to our proposal is both initiated and catalyzed by ammonia (and methyl amines) where hydrogen bonding between the amines and the polymer nitrogen side groups plays a crucial role in conducting the ammonia molecules to the reaction center before evaporation and thus loss of the ammonia) leading to moieties such as **b** and **c** in Scheme 1. These moieties were detected by means of sophisticated solid-state NMR spectroscopic methods. The second sub-branch of **A** is, according to our proposal, a Diekmann-analogous reaction followed by a reaction cascade that we already have proposed in a previous paper.[21] Pathway **A** also offers an explanation for the unequivocally found formation of water during the thermal treatment, ending up with structure motifs such as **a**, **d**, **d′** and **d″** which are again supported by our solid-state NMR study.

Along the second main reaction pathway **B** no methanol and no water is released. We propose a reaction cascade of a Ziegler/Thorpe-analogous reaction, followed by retro-hetero-en reaction (structure motif **e** in Scheme 1), and followed partly by a Krapcho-analogous reaction (structure motif **f** in Scheme 1). The latter is responsible for the detected release of the CO_2 along with also detected methyl amine species, which are formed during the same time range. By means of solid-state NMR spectroscopy we could quantify the amount of MA^{CH3} groups still present in the thermally treated bulk material of sample P9 to about 41% while the yield of CO_2 relative to the MA content could be quantified to about 9–11% (along with about 1%–2% trimethyl amine). Thus, we conclude that in total about 50% of all thermal transformations run along the main pathway **B** at about 5 mol% MA content. This means that taking together the chemical transformations along both pathways in this range we can explain more than 90% of all changes concerning the MA repeat unit with Scheme 1.

ACKNOWLEDGMENT

Open Access funding enabled and organized by Projekt DEAL.

DATA AVAILABILITY STATEMENT

No. Research data are not shared.

ORCID

Klaus Ruhland https://orcid.org/0000-0003-0277-618X
Robert Horny https://orcid.org/0000-0003-1408-8392

REFERENCES

[1] E. Frank, F. Hermanutz, M. R. Buchmeiser, *Macromol. Mater. Eng.* **2012**, *297*(6), 493.
[2] E. Frank, L. M. Steudle, D. Ingildeev, J. M. Spörl, M. R. Buchmeiser, *Angew. Chem.* **2014**, *126*, 5364.
[3] E. Ismir, A. S. Sarac, *Polym. Adv. Technol.* **2016**, *27*, 1383.
[4] S. H. Bahrami, P. Bajaj, K. Sen, *J. Appl. Polym. Sci.* **2003**, *89*, 1825.
[5] P. Bajaj, D. K. Paliwal, K. A. Gupta, *J. Appl. Polym. Sci.* **1993**, *49*, 823.
[6] G. Venkataramana Reddy, G. Radhakrishnan, *Angew. Makromol. Chem.* **1984**, *121*, 41.
[7] H. Kakida, K. Tashiro, *Polym. J.* **1997**, *29*(4), 353.
[8] R. Devasia, C. P. Reghunadhan Nair, P. Sivadasan, B. K. Katherine, K. N. Ninan, *J. Appl. Polym. Sci.* **2003**, *88*, 915.
[9] R. Devasia, C. P. Reghunadhan Nair, R. Sadhana, N. S. Babu, K. N. Ninan, *J. Appl. Polym. Sci.* **2006**, *100*, 3055.
[10] Z. Wangxi, L. Jie, W. Gang, *Carbon* **2003**, *41*, 2805.
[11] G. Radhakrishnan, T. Nagabhushanam, K. T. Joseph, M. Santappa, *Makromol. Chem.* **1979**, *180*, 2923.
[12] J. Simitzis, *Colloid Polym. Sci.* **1977**, *255*, 1074.
[13] J. Simitzis, *Colloid Polym. Sci.* **1977**, *255*, 948.
[14] G. S. Bhat, L. H. Peebles Jr., A. S. Abhiraman, F. L. Cook, *J. Appl. Polym. Sci.* **1993**, *49*, 2207.
[15] H. Ogawa, *Chem. Soc. Jpn.* **1994**, *5*, 464.
[16] Y. H. Bang, S. Lee, H. H. Cho, *J. Appl. Polym. Sci.* **1998**, *68*, 2205.
[17] P. Rangarajan, J. Yang, V. Bhanu, D. Godshall, J. McGrath, G. Wilkes, D. Baird, *J. Appl. Polym. Sci.* **2002**, *85*, 69.
[18] V. A. Bhanu, P. Rangarajan, K. Wiles, M. Bortner, M. Sankarpandian, D. Godshall, T. E. Glass, A. K. Banthia, J. Yang, G. Wilkes, D. Baird, J. E. McGrath, *Polymer* **2002**, *43*, 4841.
[19] D. Godshall, P. Rangarajan, D. G. Baird, G. L. Wilkes, V. A. Bhanu, J. E. McGrath, *Polymer* **2003**, *44*, 4221.
[20] J. Zhao, J. Zhang, T. Zhou, X. Liu, Q. Yuan, A. Zhang, *RSC Adv.* **2016**, *6*, 4397.
[21] K. Ruhland, R. Frenzel, R. Horny, A. Nizamutdinova, L. van Wüllen, J. Moosburger-Will, S. Horn, *Polym. Degrad. Stab.* **2017**, *146*, 298.

[22] K. Ruhland, F. Habibollahi, R. Horny, *J. Appl. Polym. Sci.* **2020**, *137*(6), 48357.
[23] L. C. Leitch, *Can. J. Chem.* **1957**, *35*(4), 345.
[24] C. Azuma, M. L. Dias, E. B. Mano, *Makromolekulare Chemie. Macromolecular Symposia*, Vol. 2, Hüthig & Wepf Verlag, Basel **1986**, p. 169.
[25] A. K. Gupta, R. P. Singhal, *J. Polym. Sci.* **1983**, *21*, 2243.
[26] J. P. Bell, J. H. Dumbleton, *Text. Res. J.* **1971**, *41*, 196.
[27] B. Wang, S. Xiao, W. Cao, X. Shi, L. Xu, *J. Appl. Polym. Sci.* **2012**, *124*, 3413.
[28] M. Bak, J. T. Rasmussen, N. C. Nielsen, *J. Magn. Reson.* **2000**, *147*, 296.
[29] W. Kolodziejski, J. Klinowski, *Chem. Rev.* **2002**, *102*, 613.
[30] D. Massiot, F. Fayon, M. Capron, I. King, S. Le Calve, B. Alonso, J.-O. Durand, B. Bujoli, Z. Gan, G. Hoatson, *Magn. Reson. Chem.* **2002**, *40*, 70.
[31] T. Gullion, *Concepts Magn. Reson.* **1998**, *10*, 277.
[32] Y. Pan, T. Gullion, J. Schaefer, *J. Magn. Reson.* **1990**, *90*, 330.
[33] L. van Wüllen, G. Tricot, S. Wegner, *Solid State Nucl. Magn. Reson.* **2007**, *32*, 44.
[34] A. P. Krapcho, J. F. Weimaster, J. M. Eldridge, E. G. E. Jahngen Jr., A. J. Lovey, W. P. Stephens, *J. Org. Chem.* **1978**, *43*(1), 138.
[35] A. P. Krapcho, E. G. E. Jahngen Jr., A. J. Lovey, *Tetrahedron Lett.* **1974**, *13*, 1091.
[36] A. P. Krapcho, G. A. Glynn, B. J. Grenon, *Tetrahedron Lett.* **1967**, *3*, 215.
[37] F. Texier, E. Marchand, R. Carrie, *Tetrahedron* **1974**, *30*, 3185.
[38] E. J. Parish, B.-S. Huang, D. H. Miles, *Synth. Commun.* **1975**, *5*(5), 341.
[39] D. H. Miles, B.-S. Huang, *J. Org. Chem.* **1976**, *41*(2), 208.

SUPPORTING INFORMATION

Additional supporting information may be found in the online version of the article at the publisher's website.

How to cite this article: K. Ruhland, R. Horny, A. Wanzel, S. Reisach, A. Nizamutdinova, H. Kirchhain, U. Rehfuss, L. van Wüllen, A. Fischer, F. Scheliga, T. Hübner, *J. Appl. Polym. Sci.* **2022**, *139*(18), e52074. https://doi.org/10.1002/app.52074